Responses to reviewer's comments for “Dynamical and hydrological changes in climate simulations of the last millennium”

We are grateful to the reviewers for their comments and suggestions, all of which have been helpful for improving the manuscript. We respond to each of the comments in our thorough replies below, providing in gray the comments from each review and in black our responses. Line and figure numbers correspond to the lines and figures in the newly revised manuscript unless otherwise noted.

Reviewer 1:

R1C0

In this manuscript the authors analyse in a multi-model framework the typical responses of different key climate variables to the changes in the radiative forcing that occurred during the last millennium. This is nicely done by concatenating a large set of CMIP5/PMIP3 simulations, and computing the leading EOFs for several variables that describe different thermal, dynamical and hydrological aspects of the climate system. Since all concatenated simulations are driven with past estimates of the external radiative forcings, which synchronise some of the climate excursions across the different experiments, the EOFs extracted from the ensemble tend to successfully represent the common forced signal to all simulations. The analysis explores separately the long-term responses due to both anthropogenic and natural radiative forcing factors, as well as the short-term impact of the largest volcanic eruptions. I find the multi-model approach to be original and insightful, and the results of great interest. I thus recommend a minor revision of the manuscript, and enclose a list of comments that the authors would need to address to render the article suitable for publication in Climate of the Past.

Following the comments from the reviewers, important changes have been done in the text to reduce its length (R1C1, R1C17 and R1C21), remove misleading statements (R1C36, R2C14, R2C15 and R2C16), and include the assessment of NAO, NAM and SAM indices (R1C2, R1C26 and R2C12), maps of climatology for SLP, zonal wind and precipitation (R1C26, R1C28 and R1C34), and the significance of SEA and the analyses of monsoon domains (R1C3 and R1C35).

General Comments:

R1C1

1. The article is rather lengthy, and some parts feel repetitive. It would certainly benefit from some synthesis effort, so that the key messages are not obscured by the details. Some Figures could be removed, and their specific discussion in the main text shortened. For example, the most important changes in the hydrological cycle could be well described with just two variables: precipitation and the drought severity index. The P-E patterns are really close to those of precipitation (suggesting that precipitation is the dominant contributor to the surface freshwater fluxes over the continents). And soil moisture, as the authors already acknowledge in the paper, is not the most appropriate variable for inter-model comparison because different models compute it differently. And besides, it does not show a clear significant response to the forcings.

Even if it is not the main contribution of the paper, the comparison of different variables representative of the hydroclimate, and in particular of the water content of the soil (P-E, scPDSI and soil moisture), is from our point of view an interesting result. Indeed, one conclusion from these analyses is that P-E is mostly affected by precipitation and PDSI by temperature, while soil moisture is very model-dependent. This is something that could be taken into account for future analyses based on the simulated hydroclimate. This follows an emerging convention to analyze a comprehensive suite of drought indicators, as done in other studies focused on drought projections

(Cook et al.,2020). We have tried to make this more clear in the new version, and hope the reviewer finds it convincing.

Regarding the length of the paper, we have removed the first paragraph of sections 3.1 and 3.2, according to comments R1C17 and R1C21. Following the same approach, we have removed those paragraphs with redundant information, including the sixth of section 3.2 and the first of section 3.3.

R1C2

2. The global patterns of response (both the EOF and MCA-LIA composites) are beparticularly useful, as they help to easily identify the regions with the largest responses. But not so much the analyses based on zonal averages of dynamical and hydrological variables (Figures 8a and 11c), for which many of the regional features of the response are smoothed out. Indeed, it would be more interesting to address directly the response of the key indices that control these regional changes (ENSO/PDO, NAO, SAM,...). Plotting their associated time series, like in Fig 13, would allow to see how robust their forced signals across simulations are.

To better represent the changes from MCA to LIA and its associated significance, several changes have been performed in the new version. Contours with climatology have been added to MCA-LIA maps according to comments R1C28 and R1C34, analyses of the latitudinal distribution of temperatures have been included in R1C20, significance of the changes in moonson domains have been added and commented according to R1C31 and R1C35, and changes in the text have been done in agreement with R1C23, R1C25 and R1C30. In this context, Fig. 9b and 12c show latitudinal changes that are useful to understand the impact of external forcing. The text associated with these figures has been changed to clarify its relation with the NAO, NAM and SAM indices: (P17 L14 - P18 L3) "*During the simulated MCA, changes in zonal and meridional winds took place with anti phase relationships that strengthened the zonal circulation at mid and high latitudes (Fig. 9b) with increases in the NAO, NAM and SAM (Fig 5), while within the intertropical regions the Trade winds and convergence were intensified (Fig. 7c and Fig. 9).*"

To support the discussions related to the NAO, NAM and SAM phenomena in Sect. 3.2, the associated indices have been computed and the percentage of positive phases for 50-year intervals has been included in Fig. 5. This figure shows a larger percentage of positive phases for the three indices during the MCA and industrial period, indicating significant changes in the zonal circulation. The text has been modified accordingly: (P15 L4-8) "*This pattern is associated with an intensification (MCA) and weakening (LIA) of the SAM and NAM/NAO, as shown in Fig. 5. The figure shows the percentage of years with positive NAO, NAM and SAM indices for successive intervals of 50 years. Consistent with the spatial patterns and temporal evolutions shown in the PC analysis, a tendency toward more positive phases of the NAO, NAM and SAM is observed during the MCA and industrial periods.*"

A description of how the NAO, NAM and SAM indices have been computed has been included in the methods section: (P10 L3-11) "*To better analyse the changes in the extratropical zonal circulation, the NAO, NAM and SAM indices have been computed. The NAO index has been obtained (Stephenson et al., 2006) with the difference of boreal winter (December, January and February; DJF) SLP average for (90°W to 60°E, 20°N to 55°N) and (90°W to 60°E, 55°N to 90°N), the NAM index was calculated (Li and Wang, 2003) as the difference between the DJF zonal mean SLP at 35°N and 65°N, and the SAM index was calculated from the difference between the zonal mean of annual SLP at 40°S and 65°S (Gong and Wang, 1999). The NAO, NAM and SAM indices have been obtained for each simulation in Table 1. The average of all the simulations was subsequently computed to determine the percentage of years with positive phases for successive intervals of 50 years. The change in the percentage of positive phases from the MCA to LIA was in* *turn assessed and the significance of the changes evaluated using a student t-test.*"

R1C3

3. The volcanic impact analysis has also room for improvement. On one hand, it is currently focused on the global mean response, which makes sense for temperature (a variable that responds directly to changes in the radiative forcing), but not so much for the dynamical and hydrological variables, whose response is, as I already mentioned, more regional. Focusing the plots on the regions with the largest response, as identified by the EOF or MCA-LIA composites, would help to identify stronger and more persistent influences of the volcanic eruptions to those in the global means. On the other hand, the current volcanic analysis is missing some estimate of statistical significance, which is essential to identify whether those responses are indeed meaningful. This could be done with a bootstrap approach that scans the periods with no volcanic eruptions to establish the significance threshold.

The spatial distribution of SLP and zonal wind during volcanic events are respectively shown in Fig. 6 and Fig. 8. In these figures, it can be observed that for most regions the pattern resembles that of the EOF. The analysis of volcanic events is mainly focused on the global scale, but these analyses show that the impact of volcanic events is similar to that of the external forcing factors in the long term, and the spatial patterns obtained with the EOFs are therefore representative of the behavior during these events.

Regarding the significance of changes during volcanic events, we have added the significance level to Figures 2d, 4d, 7d, 11d, 15d, 16d and 17d, obtained with a bootstrap approach, by computing the percentile 5 and 95 of the distribution of averages generated with 2200 sets of 12 years (100 for each simulation) randomly selected from the whole period, excluding the years of volcanic eruptions and the ten years after them.

The description of this approach has been also included in the methods section: (P6 L3 - P7 L2) "*The significance of the changes in the variables evaluated within the SEA has been calculated using a bootstrap method. 2200 sets of 12 years (100 for each simulation) have been randomly taken from the whole analysed period, excluding the years of volcanic eruptions and the ten years after them, to generate a distribution of averages for each variable. The significance of the averages computed after the 12 volcanic eruptions are then determined using the 5 and 95 confidence limits from the bootstrap distribution.*"

Specific comments:

R1C4

- Page 2 Line 2: responses → changes

Changed.

R1C5

- Page 2 Line 5: consistently → consistent

Changed.

R1C6

- Page 3 Line 1: also have been → have also been

Changed.

R1C7

- Page 3 Line 10: the CMIP5/PMIP3

Changed to “*CMIP5/PMIP3*”.

R1C8

- Page 3 Lines 14-15: “, the Meteorological. . ., and with 13” → “and the Meteorological. . ., and 13l”

Changed.

R1C9

- Page 4 Figure 1 caption/Page 5 Line 10: composing → aggregating

Changed.

R1C10

- Page 5 Lines 28-30: The phrasing is confusing. I didn’t really understand how it’s done until I saw Figure 2d. The sentence suggests that compositing (or averaging) is not done with the five years before and 10 years after the volcanos, but it is instead done over the 12 main volcanic eruptions. And this is done for every year from the 5 preceding to the 10 following those volcanic eruptions.

The paragraph has been rephrased to: (P5 L31-33) “*To assess the impact of such events on the climate, we use a Superposed Epoch Analysis (SEA), by defining a composite with the main volcanic eruptions within the LM and computing for this composite the global average of the variables previously mentioned for the five years before and ten years after the events*”

R1C11

- Page 5 Lines 31-33: Could you explain why is Gao’s forcing used in some comes, and Crowley and Unterman’s in others?

The idea is to use for the definition of the composite the dates of the largest eruptions that correspond to the actual forcing used for the simulation itself. The simulations of CESM-LME and CCSM were generated using Gao's forcing, so we considered more suitable to use this forcing also for the definition of the composite. In the other simulations, we selected Crowley and Unterman's forcing, as done in Masson-Delmotte et al. (2013).

We have made changes in the text to clarify this: (P5 L34 - P6 L1) “*For simulations of CESM-LME and CCSM, which use the reconstruction from Gao et al. (2008) as volcanic forcing, the years of the composite have been selected based on the minima of forcing from this reconstruction: 1452, 1584, 1600, 1641, 1673, 1693, 1719, 1762, 1815, 1883, 1963 and 1990.*”

R1C12

- Page 6 Table 2 Caption: temperature → surface temperature; of each → for each

Changed.

R1C13

- Page 6 Lines 1-3: Could you clarify if to make the multi-model concatenated array in which the EOF’s are computed you first regrid all the experiments to a common grid? And to which one in that case? Otherwise the EOF array would be irregular in time. Or have the simulations been concatenated in space?

Yes, the simulations have been regrided to a common grid before concatenating them. This procedure is explained in Sect. 2: (P5 L28-29) "*All simulations have been interpolated to a common 6ºx6º grid resolution, the coarsest among the analysed simulations.*"

R1C14

- Page 6 Line 4: Do you really apply an average? Or is it simply the EOF of the concatenated simulations? If there is no averaging it is better to refer to it as the "multi-model EOF".

The multi-model EOF is not an average of the individual EOFs. We have removed the term "average EOFs", as it may be misleading.

We filter out the high frequency variability to focus on the low frequency response to external forcing by applying prior to the EOF analysis a 31-year running mean low pass filter, also as in previous work by the group (Fernandez-Donado et al 2013). Slight changes have been made to clarify this: (P7 L5-6) "*We concatenate all of the low-pass filtered simulations to determine the Empirical Orthogonal Functions (EOFs) across all of the models.*"

R1C15

- Page 7 Line 4: It would be more clear if you change "resulting EOFs" for "single experiment EOFs" Also, to prove that the differences are minor, you could compute the spatial pattern correlations between the individual EOFs and the multi-model one, and provide the range of correlation values in the text.

Spatial correlations between single experiment EOFs and multi-model EOFs have been added: (P8 L5-7) "*The single experiment EOFs bear only regional differences that do not contradict the results obtained with the combined analyses, with spatial correlations with the multi-model EOFs reaching 0.9 for some simulations and 0.7 for most of them.*"

R1C16

- Page 8 Figure 3 Caption: Also for clarity I would change "a PC analysis" → "the multi-model EOF analysis"

Changed.

R1C17

- Page 8 Lines 9-17: It feels weird to start your result section with a paragraph revising previous results. That's what the introduction is for. Previous results can also be discussed in the results section as well, but to contrast with your findings once they have been introduced. I strongly recommend to start directly with the second paragraph.

The paragraph has been removed. The definition of MCA and LIA according to Masson-Delmotte et al. (2013), which was included in that paragraph, has been moved to the previous section, since it is needed to understand the selection of years for the composites.

R1C18

- Page 9 Lines 11-12: Not sure I agree. There are still important differences across members with the same model, which are hard to discern given the high line density in Figure 1c. To compare appropriately the forced vs internally driven temperature changes you would need, for a specific model ensemble, to compute the ensemble mean (which would describe the forced signal) and remove it from each of the individual members (to extract its internal variability component). I expect that many centennial changes will be of similar magnitude than the MCA-LIA transition. The exception should be the industrial warming trend, which will most probably remain unparalleled.

Thank you, this was a very useful suggestion. The internal variability component has been estimated by removing the ensemble average from each ensemble member. The results are included in Fig. R1.

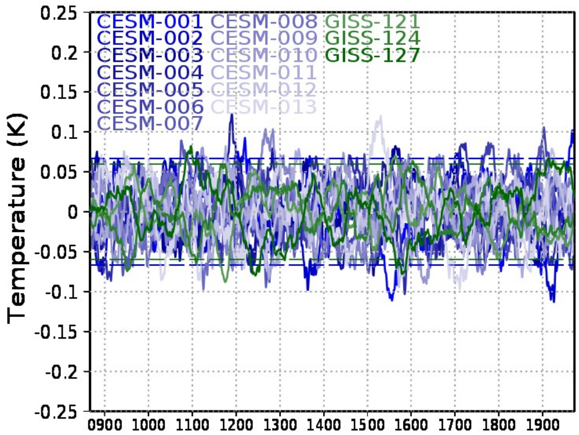

Figure R1. Differences between each ensemble member simulation in Fig. 1c and the corresponding ensemble average. Dashed lines show $\bar{x} \pm 2s$ where $\bar{x}$ is the long-term mean of the residuals (zero) and *s* the standard deviation.

Dashed lines in Fig. R1 show plus-minus the value of the residual standard deviation in the test suggested by the reviewer. The text has been modified accordingly: (P10 L22-31) "*These subensembles demonstrate that internal variability generates differences across simulations that are smaller than structural differences in model formulation across models. Figure 1c shows the range (dashed lines) of the residuals resulting from substracting the ensemble mean from each ensemble member simulation. Since the average of all ensemble members cancels out uncorrelated contributions of internal variability, the resulting ensemble mean constitues a smoothed estimation of the forced response and the residuals of substracting the ensemble mean from each ensemble member is an estimation of internal variability above 31-year timescales (Crowley, 2000; PAGES2k-PMIP3 group, 2015). Both the CESM and GISS ensembles in Fig. 1c show pre- and post-1850 low frequency changes larger than the estimated changes of internal variability. Changes in the ensemble associated with external forcing are therefore in general more relevant than those of internal variability above 31-year timescales.*"

R1C19

- Page 9 Lines 27-29: I suggest rephrasing the second sentence to make clear that polar amplification is characteristic of the sea ice covered regions (via ocean/sea ice albedo feedbacks, among other processes) but not of the continental areas.

The paragraph has been rephrased: (P11 L13-15) "*Regarding the spatial pattern of the EOF, values are larger over continental regions and smaller over oceans. For high latitudes, larger values are obtained over ice covered areas, consistent with the polar amplification response in climate change scenarios*"

R1C20

- Page 9 Lines 32-34: There is an important qualitative difference between Figure 2a,c that the authors do not comment. In the EOF, there is a stronger response in the Tropics than in the subtropics, that does not occur during the MCA-LIA transition. Could the authors discuss it, and the potential reasons?

The difference is related to the different timescales of variability in tropical and extratropical areas. The tropical areas are more affected by high frequency variability, which is included in the EOF but not in the map of MCA-LIA differences that emphasize low frequency changes. This can be shown with the time series of temperature for different latitudes in Fig. R2. It can be observed that for extratropical areas the differences between the MCA and LIA are much larger than in the tropics.

a) High Southern Latitude

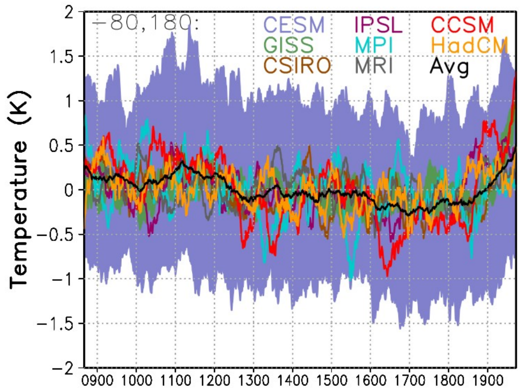

b) Extratropical Southern Latitude

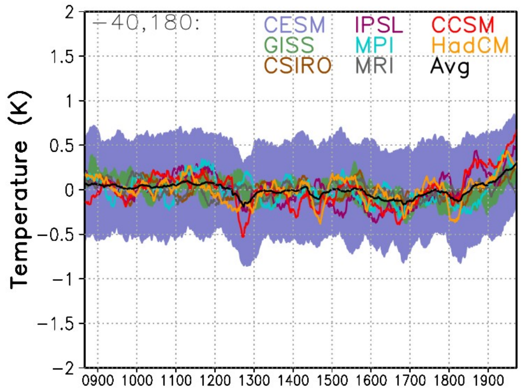

c) Tropical Latitude

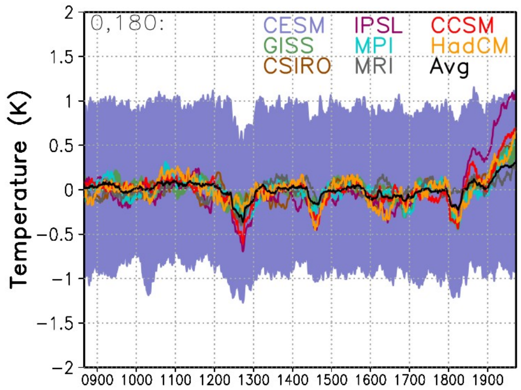

d) Extratropical Northern Latitude

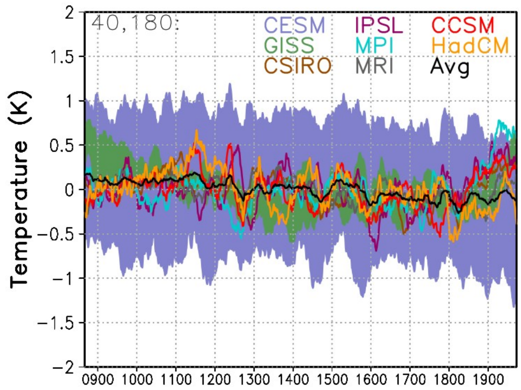

e) High Northern Latitude

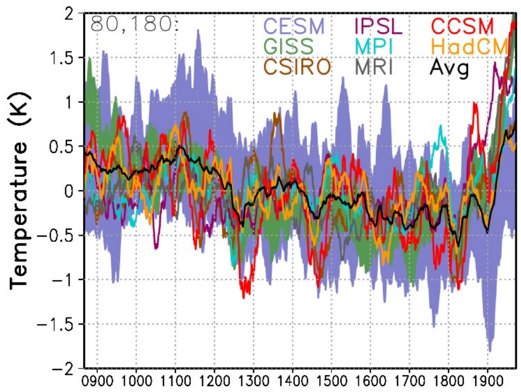

Figure R2. Time series of temperature for locations at different latitudes in the Pacific basin: **(a)** (-80º,180º), **(b)** (-40º,180º), **(c)** (0º,180º), **(d)** (40º,180º) and **(e)** (80º,180º).

The text has been modified to include this clarification: (P11 L19-22) "*The MCA-LIA pattern does* *not emphasize the tropics as much as the EOF pattern, indicating that the low frequency variability changes in that area are minor and the higher tropical loadings in Fig. 2a stem from covariability at higher frequencies. Also note that area weighting has been applied for the EOF calculations, increasing the contribution of the tropical areas in these analyses.*".

R1C21

- Page 10 Lines 7-8: Same as before. You start a subsection of results describing previous literature. Also, please note that the two modes of internal variability that you mention explicitly (ENSO and PDO) are coupled modes that involve the ocean, and therefore only partly related to atmospheric dynamics. It would make more sense to put forward the NAO, which is purely atmospheric and has been studied during the last millennium with different proxy reconstructions.

The paragraph has been removed, since this information is already included in the introduction.

R1C22

- Page 11 Lines 5-6: Could you specify what you mean by long term behaviour? The first PCs of SLP are basically characterised by a flat line and a positive trend starting in 1700. By contrast, the respective ones for surface temperature include strong multi-centennial oscillations, which for some models are of similar magnitude than the industrial warming trend.

The explanation is included in the next sentence: (P11 L32-33) "*For the case of pressure, the average PC (black line in Fig. 4b) tends to show higher values during the MCA, lower during the LIA and a significant increase during the last century.*". The average PC in Fig. 4b shows larger values during the MCA than during the LIA. More details can be found in R1C27 and Table R1.

R1C23

- Page 11 Line 6-7: I wonder if the MCA-LIA difference that can be seen in Figure 4b is really significant. It does not seem to occur consistently for all the models. Indeed, another indication that the MCA-LIA difference is not a remarkable feature comes from the spread of correlations across model PCs in Figure 4b, which are only clearly above zero if the industrial era is considered.

The level of significance of the MCA-LIA is included in Fig. 4c. It shows significant changes for broad regions in northern latitudes (negative) and the tropics (positive). The significance of the PC correlations is also discussed in the text. Indeed MCA-LIA changes in SLP may be more subject to internal variability than temperature. Some changes have been made in the text to better represent the results: (P11 L31-33) "*The long-term behaviour of the first PC of pressure is comparable to that of the first PC of temperature. For the case of pressure, the average PC (black line in Fig. 4b) tends to show higher values during the MCA, lower during the LIA and a significant increase during the last century.* "

R1C24

- Page 11 Line 17: What do you mean by SLP stratification? Do you refer to the typical zonally-symmetric dipolar SLP response of SAM to global warming, with relative low surface pressure conditions at subpolar latitudes and high conditions at polar latitudes?

Yes, the text has been modified to make this clear.

R1C25

- Page 12 Line 3: There is not such a good similarity in the Southern Hemisphere. Note for example that over Antarctica the response is of the opposite sign in the MCA-LIA pattern than in the EOF.

Changed to: (P15 L1) "*As in the leading EOF, the spatial pattern of the MCA-LIA differences (Fig.*

4c) also emphasizes the latitudinal gradients".

R1C26

- Page 12 Lines 4-5: The SAM intensifications/weakenings during the MCA/LIA are far from evident from Figure 4c. In particular, the significant response is not zonally-symmetric, and as mentioned before, Antarctica experiences a relative high during the MCA. If you really want to prove that MCA-LIA transition was accompanied by a weakening of the NAO/SAM, you should do show it with their respective indices.

Climatological SLP has been added to Fig. 4c, according to R1C28. This shows that positive MCA-LIA differences appear over the maxima of SLP and negative differences over the minima, reinforcing the zonal circulation and contributing to more positive phases of the SAM.

As noted in R1C2, the NAO, NAM and SAM indices have been computed and the percentage of positive phases has been included in Fig. 5. For the three indices, a larger percentage of positive phases is obtained during the MCA and a smaller percentage during the LIA, indicating intensifications and weakenings, respectively.

The text has been modified accordingly: (P13 L5 - P14 L1) "*This spatial pattern, with positive loadings over the maxima of climatological SLP (black contours of Fig. 4a) and negative loadings over the minima (green contours of Fig. 4a), contributes to the positive phase of the mode to intensify gradients between subtropical and subpolar regions. This reinforces zonal circulation and contributes to more positive phases of the SAM (Jones et al., 2009; Fogt et al., 2009), as shown in Fig. 5.", (P14 L2-5) "Overall, higher positive (negative) loadings distribute over subtropical (polar) regions contributing to increase (decrease) the zonal flow during the MCA and industrial period, due to the slightly higher values of the PC, also consistent with NAM (Thompson and Wallace, 2001) enhancement.*"

R1C27

- Page 13 Lines 32-34: There is no evident change from MCA to LIA in the PCs of the zonal wind. This implies that the EOF pattern mostly reflects the changes during the industrial period but not during the MCA.

The changes from MCA to LIA in Fig.7b are evident in a decrease in the average PC (black line). Table R1 shows the difference in the average PC of temperature, SLP, zonal wind and precipitation between the MCA and LIA and the associated significance level ($p<0.05$). It can be seen that for all the variables the changes in the average PC from MCA to LIA are significant.

Table R1. Differences between MCA and LIA from the average PC time series of Fig. 2b, 4b, 7b and 11b. Significance level ($p<0.05$) is also included, obtained with a t-test for the difference of averages accounting for autocorrelation.

Variable	**MCA-LIA**	**Significance level (p<0.05)**
Temperature	1.12	0.33
SLP	0.24	0.16
Zonal wind	0.16	0.14
Precipitation	0.62	0.18

As discussed in R1C20, the MCA-LIA map emphasizes the low-frequency changes. During the MCA, subtropical westerlies are strengthened with respect to the LIA, consistent with the discussed changes in the zonal circulation (see R1C2, R1C26, R1C28 and R2C12).

R1C28

- Page 13 Lines 34-35: To know if the EOF corresponds with a poleward displacement you need to show as well the mean zonal climatological winds. Otherwise, how can you tell that positive/negative loadings do not correspond to intensifications/weakenings of the climatological winds?

Contour lines for climatological SLP, zonal wind and precipitation have been added to Fig. 4, Fig. 7 and Fig.11. The positive (negative) climatological winds in Fig. 7 show the location of the Westerlies (Easterlies). It can be seen that positive anomalies are found in the high latitude side of the Westerlies, indicating a poleward displacement.

The text has been modified accordingly: (P16 L1-4) "*In the positive phase of the mode, negative (positive) loadings tend to distribute over the Easterlies (Westerlies) and over their high latitude side, thus increasing latitudinal gradients and contributing to a polar displacement of the wind system; trade winds are enhanced towards higher latitudes in the Atlantic and eastern Pacific.*"

The linkage between loadings and climatology also has been included for the case of SLP: (P13 L5 - P14 L1) "*This spatial pattern, with positive loadings over the maxima of climatological SLP (black contours of Fig. 4a) and negative loadings over the minima (green contours of Fig. 4a), contributes in the positive phase of the mode to intensify gradients between subtropical and subpolar regions. This reinforces zonal circulation and contributes to more positive phases of the SAM (Jones et al., 2009; Fogt et al., 2009), as shown in Fig. 5*"

R1C29

- Page 15 Lines 3-5: The spatial patterns in figure 7 show also important differences that should be acknowledged. For instance, in the North and Tropical Atlantic, or in the whole Pacific region.

That is the goal of these figures and the associated paragraph, to show that there exist differences between CESM and GISS subensembles in the spatial pattern during volcanic events. The paragraph is now rephrased to provide the details of the regions with differences: (P17 L8-11) "*In spite of the differences in some areas like the North and Tropical Atlantic and Pacific basins, both subensembles tend to weaken the global zonal circulation. However, the simulations of CESM (GISS) show more areas with positive (negative) zonal winds, which translate into a larger (smaller) increase of the global average.*"

R1C30

- Page 18 Lines 9-10: Similar to the previous comment. In this case the response is really different in the Tropics.

The text has been modified following this comment: (P20 L9-12) "*The MCA-LIA differences (Fig. 11c) show some similarities with the EOF loadings in extratropical regions, indicating larger precipitation at northern latitudes in the MCA (Fig. 11c) or with increased forcing at all timescales above 31 years (Fig. 11a,b). Within the tropical regions agreement is regionally complex, with MCA-LIA differences emphasizing low-frequency changes and EOF loadings including covariability at all timescales.*"

R1C31

- Page 18 Lines 16-17: I don't understand this statement. Figure 10 shows a positive response in North America, while climate projections suggest that the response is zero.

Figure 11 shows positive and negative responses over the NAMS. The text has been modified to make it clearer: (P20 L16 - P21 L2) "*MCA-LIA differences are regional in scope and show anomalies of different sign over the North and South American Monsoon Systems (NAMS, SAMS; Cerezo-Mota et al., 2011; Christensen et al., 2013), therefore without a clear response of NAMS and SAMS. This agrees with uncertainty in climate change projections over the NAMS, with CMIP5 models producing changes in precipitation that distribute around zero (Christensen et al., 2013). The same occurs over the Australian and Maritime Continent Monsoon Systems (AMSMC; Jourdain et al., 2013). Positive values are found over the East Asia and Southern Asian Summer Monsoon areas (EAS, SAS; May, 2011; Boo et al., 2011), in agreement with scenario simulations (Christensen et al., 2013)*"

R1C32

- Page 18 Line 17: Marine → Maritime

Changed.

R1C33

- Page 19 Line 2: You are not really showing consistency, just a multi-model response (which could be dominated by certain simulations/models)

In response to R1C15 and R2C5, we confirmed that the multi-model response is not biased to any simulation or model and could be considered representative of the response of the individual models. The correlations in Fig. 11b also show a good agreement among simulations, being many of the correlations significant even for the pre-industrial period. This indicates that the pattern of MCA-LIA shown in Fig. 11c is not dominated by a few simulations but common to many of them.

In any case, the sentence refers to the consistency of the spatial patterns with those obtained in scenario simulations (Christensen et al., 2013), and not to the consistency among different model simulations. The paragraph has been changed to clarify this: (P21 L2-4) "*Even if changes are not significant over many of these regions due to the large variability of precipitation, they show a pattern of response to forcing in LM PMIP3 simulations consistent with that of scenario simulations; consistency also extends to convergence zones.*"

R1C34

- Page 20 Lines 1-2: As previously mentioned for the SLP patterns, shifts can only be diagnosed in relation to a climatological state, which has not been shown nor discussed.

Following comment R1C28, contours of climatological SLP, zonal wind and preciptiation have been added to Fig. 4, Fig. 7 and Fig.11. The climatological maxima of precipitation in Fig. 11 show that, over South America, the anomalies north of the maximum are negative and south of the maximum are positive. This indicates a shift of the rainfall, as discussed in the text.

The text has been modified to clarify this: (P21 L4-6) "*Over South America, negative anomalies are found in the northwest of the climatological maxima and positive anomalies in the southeast (Fig. 11a), depicting rainfall shifts in the South Atlantic Convergence Zone (Cavalcanti and Shimizu, 2012).*"

More details can be found in R1C2, R1C26 and R1C28.

R1C35

- Page 20 Lines 4-5: The distribution is clearly centered at zero for all regions but EAS and SAS. For SAF there is a slight tendency to more positive values, but it could be happening by chance. A significance assessment would be helpful to draw more robust conclusions. You could, for instance, test if the median of the distribution is significantly different than zero.

Significance has been added in Fig. 12b. Text has been changed accordingly: (P22 L12-13) "*The largest impact of MCA-to-LIA transition in the monsoon systems appears over Asia, where EAS and SAS are significantly altered.*"

R1C36

- Page 20 Line 30: Strong statement. CCSM, HadCM , MRI and MPI don't really support this.

The statement has been changed to (P22 L35) "*Most model simulations correlate with external forcing over the same large-scale regions*"

R1C37

- Page 20 Line 35: There is no real agreement in the big picture in figure 12. Every model tends to have a different area of influence, which is particularly evident in the negative correlations.

The text has been modified as follows: (P23 L5 - P24 L1) "*Despite most of the models showing positive correlations in the extratropical and tropical areas of the Pacific basin, and negative correlations in tropical areas of the Atlantic basin and in Southeastern Asia, the areas of high correlation are spatially constrained to regional and even local scales and may not overlap in different models or even in simulations of the same model. These regional differences are likely the sign of the important influence of internal variability.*"

R1C38

- Page 24 Line 30: are → have

Changed.

R1C39

- Page 25 Lines 11-12: I find the phrasing of this sentence confusing. It's not clear if you refer to the covariability of all variables (including surface temperature) with the changes in the forcings or if you refer to the covariability between the PC related to the forcing of surface temperature, and the equivalent PCs for the other variables. I would simplify it just saying that "PC analysis was used to identify the multi-model typical pattern of response of different variables to the external forcing changes from decadal to multidecadal timescales"

Changed.

R1C40

- Page 26 Line 11: How can you tell that the hydrological is enhanced? Figures 14-17 simply show how the EOF of the forced modes of variability are, with regions of increased and regions of decreased precipitation.

The fact that the hydrological cycle is enhanced in situations of higher forcing can be observed in the EOF (Fig. 11a) and the map of MCA-LIA differences (Fig. 11c), where positive values are obtained mostly for monsoon and convergence areas where the climatological precipitation is larger (see also R1C34). Conversely, in analyses of volcanic eruptions (Fig. 11d), in which forcing is reduced, the global average of precipitation is also reduced.

This explanation is included in the text: (P22 L27-31) "*The responses described for different timescales in Fig. 11 are consistent with changes in scenario simulations described in Christensen* *et al. (2013): increases in external forcing strengthen the hydrological cycle, enhancing zonal circulation in extratropical regions and increasing the global monsoon activity and equatorial convergence. This is found in the global average of precipitation after volcanic events and in the alteration of monsoons and latitudinal distribution obtained in the EOF, indicating a relevant response to external forcing in precipitation.”*

This behavior can be more clearly shown with the time series of average precipitation for the regions with more and less climatological precipitation, as included in Fig. R3. It can be observed that for the regions of lower precipitation (lower quartile of climatological precipitation; QL), no major differences are observed between situations of higher and lower forcing, while for the regions of larger precipitation (upper quartile of climatological precipitation; QU), important changes are observed, with generally larger values during the MCA than during the LIA and with less precipitation during volcanic events. This indicates that in situations of higher forcing the precipitation increases in the regions with more precipitation, showing therefore a hydrological cycle that is enhanced. This 'wet-get-wetter' effect is consistent with that of climate change projections (Christensen et al., 2013; Huang et al., 2013).

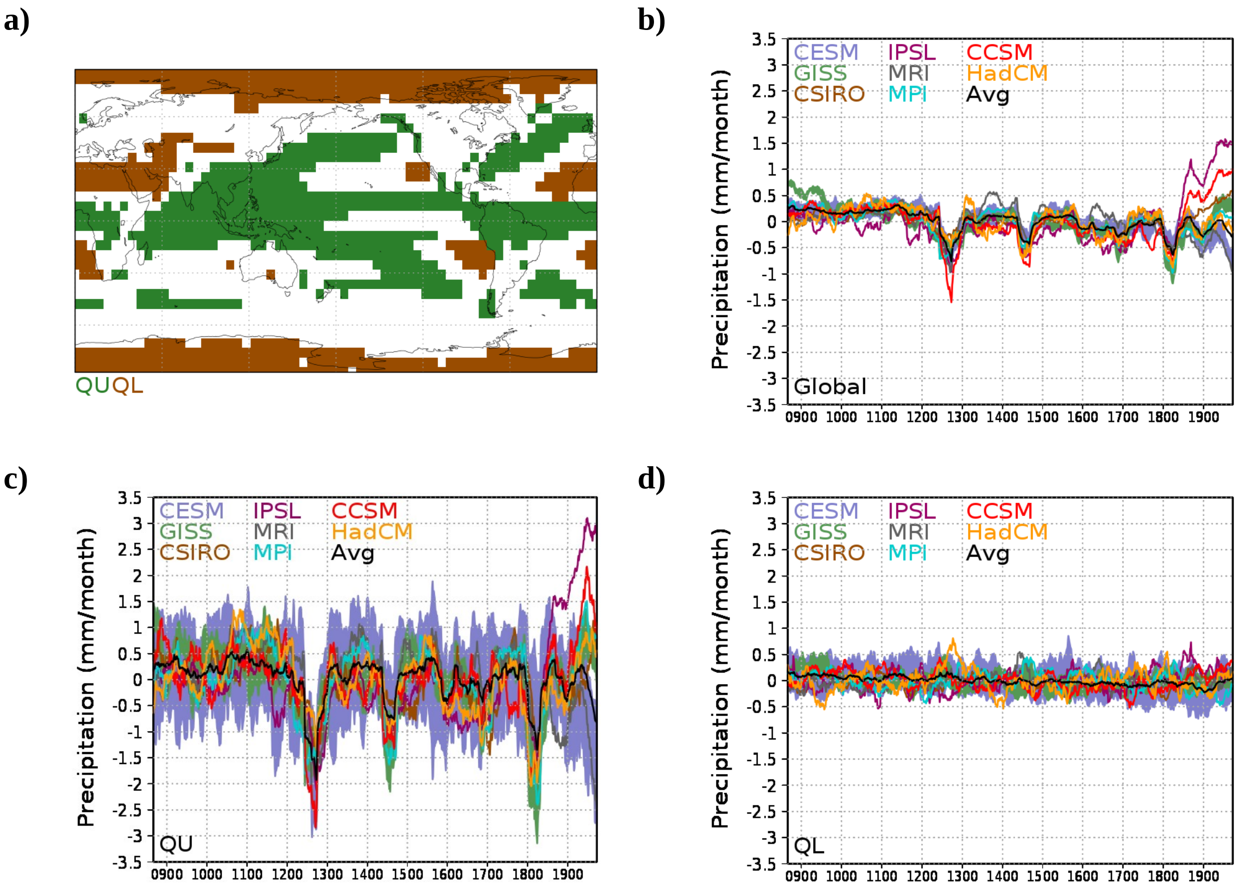

Figure R3. **(a)** Areas with climatological precipitation in the upper quartile (QU) and in the lower quartile (QL). Average of precipitation for **(b)** the whole globe, **(c)** the areas in the QU of climatological precipitation, and **(d)** the areas in the QL of climatological precipitation.

Reviewer 2:

R2C0

The paper by Roldan-Gomez and co-authors aims at evaluating the relative influence of external forcings on large-scale changes in PMIP2/CMIP5 last millennium climate model simulations including the historical period. To address this issue they relied on various statistical method and mainly EOFs analyzes and evolutions of their related PCs. Even though the paper is generally well written with potentially interesting results I have several concerns regarding the method and interpretations. The authors need to significantly improve the paper, as there are many important points to clarify or to be corrected before publication. I have listed bellow my main comments and criticism to be addressed:

We have included in the answers to the following comments clarifications and changes in the text and figures of the paper, mainly to complete the section of methods with a description of the exact experiments that have been considered for the analyses (R2C1), a more detailed description of the computation of TEF (R2C3), and a description of how the significance has been assessed at each timescale (R2C7), to remove descriptive paragraphs and statements (R1C1, R1C17, R1C21, R2C14, R2C15 and R2C16), and to include analyses based on NAO, NAM and SAM indices (R1C2, R1C26 and R2C12).

Models and methods:

R2C1

1. First of all they show time series covering the last millennium and the historical period as continuous model experiments. As far as I know this might not be the case for most of the model experiments used in this paper as the historical experiments in CMIP5 are branched off the pre-industrial control runs and are not a continuation of the LM simulations. The authors need to explain how they build the time series anomalies to make them look like seamless long climate model integrations. This is very important since this study discuss long-term trends and secular changes which depend on long term integration of external forcing histories. Historical runs branched of piControl runs might therefore include different initial mean background climate condition and trends. This should be clearly evaluated and the method used to take that into account when comparing to LM runs. How were the anomalies computed for each experiments used (piControl, LM, Historical) ?

To analyse the period from 850 to 2005 CE with CMIP5 simulations, the past1000 and historical experiments were concatenated, without performing any kind of post-processing. For some of the models (CSIRO, GISS and MPI) the historical simulations are derived from the past1000, but for others they are derived from the piControl, as indicated in the comment. This could generate a discontinuity in the input data in 1850 CE, when data from past1000 and historical experiment are concatenated. Figure R4 shows the global average of temperature, SLP and precipitation for the years between 1800 and 1900 CE, including the transition from past1000 to historical in 1850 CE. It can be observed that the discontinuity associated with the transition between experiments for these variables is not larger than the short-term variability of the data between 1800 and 1850 CE and between 1850 and 1900 CE. The impact of this transition is then removed when the short-term variability is filtered (by computing a 31-year moving average, as for the case of the analyses presented in the paper).

The text has been modified to include this information: (Table 1) "*All simulations span the period 850-2005 CE. This interval will be referred to herein as LM, even if within PMIP3 LM only includes 850-1850 CE. For the case of CMIP5/PMIP3 simulations, past1000 and historical experiments have been concatenated to cover this interval.*"

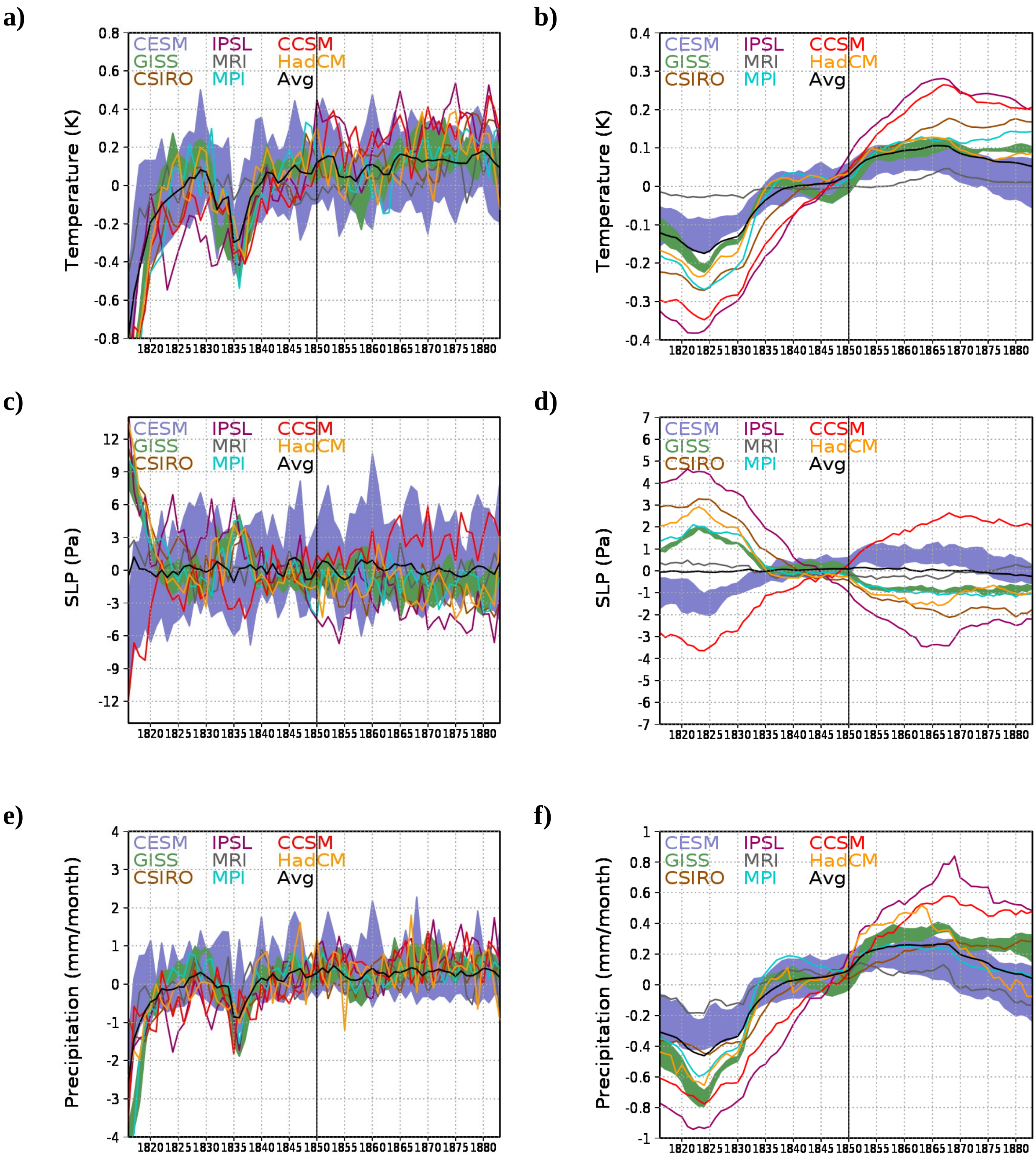

Figure R4. Global average of **(a)** unfiltered temperature, **(b)** 31-year low-pass filtered temperature, **(c)** unfiltered SLP, **(d)** 31-year low-pass filtered SLP, **(e)** unfiltered precipitation, and **(f)** 31-year low-pass filtered precipitation between 1800 and 1900 CE. The year 1850 CE, when input data changes from past1000 to historical experiments, is indicated with a vertical black line.

R2C2

2. The authors states that the model simulations were concatenated and time series low-pass filtered with a centered 31 years moving average. Which frequency cut-off was used to filter-out? The 31 years moving window was used to compute the anomalies? This should be clarified.

The only filter applied to the simulations is a 31 years moving average, which is applied to the input data before performing any analysis. This filter removes the variability in timescales shorter than 31 years. This approach has been used earlier to emphasize responses to external forcing changes

(Fernández-Donado et al., 2013; Luterbacher et al., 2016).

R2C3

3. The method used to estimate the Total External Forcing (TEF) obtained by composing the contributions of several forcing factors should be explained in the method section.

More details about how the TEF is obtained have been added in the text: (P5 L9-14) "*The figure also shows an estimation of the Total External Forcing (TEF), obtained following Fernández-Donado et al. (2013) by aggregating the contributions of solar activity, orbital changes, volcanic activity, GHGs, including CO2 , CH4 and N2O, land use change, and anthropogenic sulfate aerosols, converted into radiative forcing units and filtered with a moving average of 31 years. Even if it presents some limitations in the conversion of volcanic forcing and the contribution of aerosols (Fernández-Donado et al., 2013), the TEF allows analyses of the long-term evolution of the overall incoming energy*"

A complete description is included and discussed in Fernández-Donado et al. (2013).

R2C4

4. This section does not give enough specific and explanations as how the EOFs analyzes is developed across PMIP3 models used. How the PC selection linked to the forcing is done? Which statistical method did you consider to evaluate the spurious results related to the different forcing data-sets and implementation strategies?

To identify the PCs of each variable that are associated with the forcing we computed the correlation coefficients between all the PCs and the first PC of temperature, and selected those showing a larger correlation. The use of the first PC of temperature instead of the forcing time series removes the dependency on the particular reconstructions of forcing factors used by each model simulation. To ensure that the first mode of temperature is associated with the forcing, the correlations between the PCs of temperature and the time series of TEF for that model were also computed. These correlations and their significance are included in Table 2.

A paragraph has been added to explain this selection: (P9 L7-13) "*To identify which modes from those obtained in the PC analyses are capable of showing responses to external forcing, the correlation coefficients between their associated PC time series and the first PC of temperature have been computed, and only those showing the largest correlations have been analysed in detail. The use of the first mode of temperature instead of the time series of external forcing factors removes the dependency on the particular reconstructions used by each model simulation. To confirm that the first mode of temperature is linked to the external forcing for the analysed simulations, the correlation coefficient between the PC time series associated with this mode and the respective time series of TEF used for each specific model have been computed.*"

R2C5

5. In the PMIP3 ensemble simulation, some model multiple realizations are included in the analyzes. From my understanding, each model experiments are given the same weight when performing the EOF analyzes or ensemble averaging. This will tend to give mode weight to a few models. The authors state that the results are not affected by this sampling bias but they don't show and provide statistical measures in the subsequent analyzes to prove it. I suggest that a weighting is applied considering the number of experiments for each model to correct the sampling bias and make sure the results are unchanged.

Yes, in the analyses included in the paper each model experiment is considered with the same weight.

Thank you for the suggestion, it is a good way to check that the analyses presented in the paper are not biased to the CESM-LME for the fact of using more simulations of that model. We have performed the same analyses but using the same weight for each model, independently of the number of experiments. The EOFs and PCs obtained with this weighting approach are included in Fig. R5, and the correlations between these EOFs and the ones obtained by using the same weight for all the experiments (Fig. 2a, 4a, 7a and 11a of the paper) are included in Table R2.

The results are very similar for temperature and variables of atmospheric dynamics, with correlations larger than 0.85. The maps show more differences for the case of precipitation, especially for the tropical areas, but the correlations are still significant and these differences do not contradict any of the conclusions presented in the paper.

The text has been modified accordingly: (P8 L7 - P9 L2) "*The analyses have been also repeated weighting simulations so that each model would have the same influence, and the results are consistent (not shown).*"

Table R2. Correlations between the EOFs computed with the same weight for each model (Fig. R5) and the EOFs computed with the same weight for each simulation (Fig. 2a, 4a, 7a and 11a). Significant correlations ($p<0.05$) are shown in bold. Significance of correlation coefficients has been obtained with a t-test corrected for spatial autocorrelation following Dutilleul (1993).

Variable	**EOFs**	**Correlation**
Temperature	Fig. R5 and Fig. 2a	**0.98**
SLP	Fig. R5 and Fig. 4a	**0.95**
Zonal wind	Fig. R5 and Fig. 7a	**0.85**
Precipitation	Fig. R5 and Fig. 11a	**0.47**

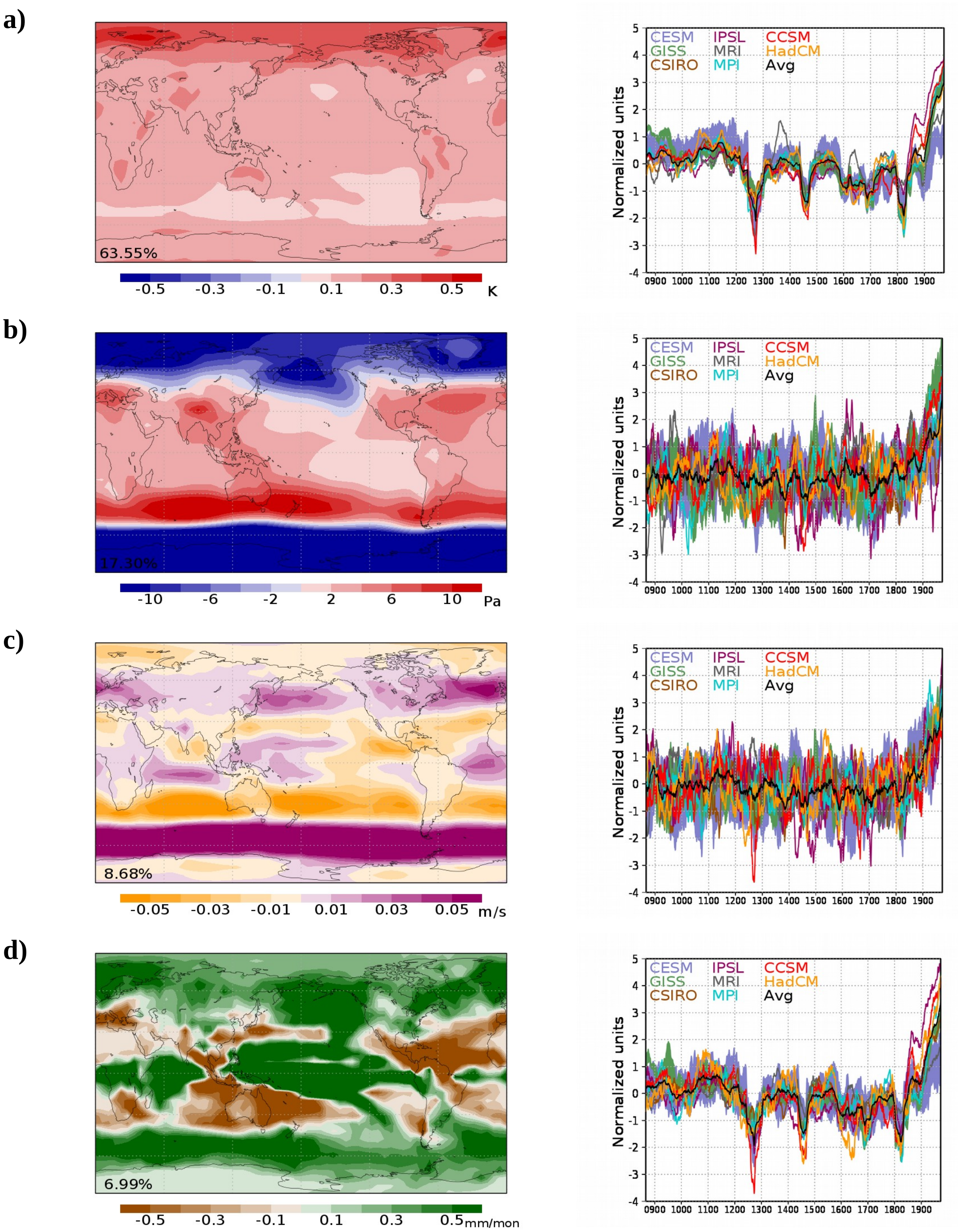

Figure R5. EOF and PC time series for each simulation, as well as the average PC of all the simulations (black line), of **(a)** temperature, **(b)** SLP, **(c)** zonal wind, and **(d)** precipitation, obtained with the same weight for each model. The percentage of explained variance is shown within the EOF map.

R2C6

6. The author state on page 8: "Some long-term changes in the external forcing, like the one during the transition from MCA to LIA, are significant enough to be obtained not only by performing PC analyzes but also by directly looking at the evolution of the variables during these two periods." I don't understand this sentence? Does that mean the authors assume that the leading PCs across LM ensemble for the considered variable and the actual evolution of the considered variable during the transition from MCA to LIA are the same? The authors should clarify this statement and prove it.

Which long term external forcing changes during MCA/LIA are the authors referring to? This statement needs to be accompanied with quantified analyzes with statistical significance estimates.

The text has been modified for clarity as follows: (P9 L15-16) "*For a more detailed analysis of the long-term changes during the transition from the MCA to LIA, composites for the MCA and LIA have been defined from the ensemble average of each variable.*"

See also R1C20 for related comments.

R2C7

Over the method section needs significant rewriting with a more systematic explanation of which methods is used to evaluated the statistical significance and relevance of the analyzes displayed in the results section. The authors should also clearly make a choice regarding the frequency window they want to investigate. Many mixed statements are presented in the results sections, regarding mean climate anomalies during the MCA relatively to LIA, secular trends and climate modes of variability occurring at various timescales. As it stands we cannot really makes sense and relate some assertion regarding climate modes of variability relying on displayed analyzes.

The text has been modified to describe in detail how the significance of changes has been assessed:

- For the SEA: (P6 L3 - P7 L2) "*The significance of the changes in the variables evaluated within the SEA has been calculated using a bootstrap method. 2200 sets of 12 years (100 for each simulation) have been randomly taken from the whole analysed period, excluding the years of volcanic eruptions and the ten years after them, to generate a distribution of averages for each variable. The significance of the averages computed after the 12 volcanic eruptions are then determined using the 5 and 95 confidence limits from the bootstrap distribution.*" More details can be found in R1C3.

- For the correlations of PCs: (P9 L13-14) "*The significance of these correlations has been assessed with a t-test for the correlation coefficient, using an effective number of degrees of freedom that considers the window of the moving average applied to the input data.*"

- For the MCA-LIA differences: (P10 L1-2) "T*he significance of these MCA-LIA differences is assesed by performing a t-test for the difference of averages between the MCA and LIA for each grid point.*" More details can be found in R1C26, R1C28 and R1C34.

- For the percentage of positive phases of NAO, NAM and SAM: (P10 L9-11) "*The change in the percentage of positive phases from the MCA to LIA was in turn assessed and the significance of the changes evaluated using a student t-test.*" More details can be found in R1C2, R1C26 and R2C12.

Regarding the analysis of different timescales, the interannual analyses with the SEA, the multidecadal and centennial analyses with the PCs, and the multicentennial analyses with the MCA-LIA differences are considered complementary. They cover the response to external forcing at a wide range of timescales.

Results sections:

R2C8

7. The authors make the following statement on page 8 in the 3.1 results section: "The peaks in volcanic forcing after the main eruptions are related to periods with lower global temperatures, while the multidecadal variability and long-term trends associated with solar and anthropogenic

forcings correspond with the long-term changes in temperatures that define periods of the MCA, LIA, and industrial era.” Which analyzes attribute the multidecadal variability and long-term trends with solar and anthropogenic forcings? This is merely assertion not proven by presented results especially with latest forcing datasets used in PMIP3 which have shown a very weak or no fingerprint of solar irradiance forcing during the LM. The authors need to provide analyzes for the multidecadal variability and trends proving otherwise.

The paragraph has been removed, following comment R1C17.

R2C9

8. Page 9: “For the 20th century, all the analyzed simulations consistently show a warming, but trends strongly differ among simulations due to the different climate sensitivities of each model and the considered forcings”. To which forcing this stronger sensitivity refers too? References should be cited to consolidate this assertion.

References have been added: (P10 L18-19) “*due to the different climate sensitivities of each model (Vial et al., 2013) and the considered forcings (see discussion in Fernández-Donado et al.,2013)*”

R2C10

9. Page 9: “In a related and most relevant note, changes in the ensemble associated with external forcing are in general more relevant than those of internal variability.” To which timescale this statement refers too? Is it for decadal or secular trends? This should be quantified and specifically quantified related to the frequency domain the authors want to discuss.

The timescale has been added, and Fig. 1c has been updated to quantify this (more details can be found in R1C18): (P10 L29-31) “C*hanges in the ensemble associated with external forcing are therefore in general more relevant than those of internal variability above 31-year timescales.*”

R2C11

10. Page 9: “Note that most of the analyzed simulations show correlations larger than 0.5 and for simulations of the same model the correlations reach values around 0.9, both when analysing the whole period and when considering only the pre-industrial era. This indicates that even if the EOF has been obtained with a combined analysis, it is also representative of the individual simulations. Additionally, the use of large sets of simulations for some of the models, and 20 in particular the use of the 13 CESM-LME simulations, does not significantly bias the results, because the correlation ranges for models with individual simulations are as large as for the others.“ Since piControl runs are a measure of internal variability for each model, I don’t understand why the authors get high correlation for both LM and piControl runs ? The method used should be clarified since the above results suggest either a flawed method or that LM changes and high correlations among model members including piControl are only due to internal variability (the leading modes of internal variability present by construction in the piControl run?).

As clarified in R2C1, piControl runs have not been used. The simulations for CMIP5/PMIP3 models extend over the past1000 (850-1850 CE) and continue over the historical (1851-2005 CE) time intervals; many of them (e.g. CESM-LME, GISS) without disruption in 1850-51. The correlations of the pre-industrial period (Fig. 2b; PRE) are therefore based on past1000 runs, while the correlations of the whole interval (Fig. 2b; ALL) are based on past1000+historical. Since the time series are low-pass filtered by a 31-year moving average, the emphasis is put on the response to external forcing (see R2C1 and R2C2 for more details).

R2C12

11. The authors also discuss changes in the leading EOF for SLP (and other hydroclimate variables)

which probably reflects the first order thermodynamical response to global temperature changes due to external forcings. Yet the authors attribute it to changes in phases of the NAO, NAM and SAM or even ENSO/IPO in response to external forcings. They don't provide any analyzes that prove it. The authors states for example that there is "a tendency toward more positive phases of the NAO, NAM and SAM is observed during the MCA and industrial periods." However no relevant analyzes are shown to sustain these statements showing for example a quantified and causal link between the leading EOF for SLP and the actual changes in (internal) variability modes. The authors rather present long-term mean anomalies between MCA and LIA or time-series of leading PCs for global scale variables. Yet by definition internal modes of variability are characterized by leading pattern and frequencies prevalence that are not analyzes in the present paper. This comment applies almost to all the points discussed in the results section where many descriptive and speculative assertion.

The PC analysis covers all the timescales from decadal to multi-centennial. The fact that the spatial patterns of the NAO, NAM and SAM appear in the EOF indicates that the first mode of SLP obtained with the PC anlaysis is showing part of the variability associated with these modes, and the associated PC time series are representative of the evolution of these modes over time. To better show these patterns, contours of climatological SLP has been added to Fig. 4a, according to R1C26, R1C28 and R1C34.

To provide more evidence of this, we have included in Fig. 5 the percentage of years with positive NAO, NAM and SAM indices for 50-year intervals. The text has been modified accordingly: (P15 L5-8) "*The figure shows the percentage of years with positive NAO, NAM and SAM indices for successive intervals of 50 years. Consistent with the spatial patterns and temporal evolutions shown in the PC analysis, a tendency toward more positive phases of the NAO, NAM and SAM is observed during the MCA and industrial periods.*" More details can be found in R1C2.

R2C13

12. For example, the presented and discussed results for SLP changes are confusing and somewhat contradictory. For instance, the authors state "simulations of GISS show an increase of pressure after volcanic events, while simulations of CESM-LME consistently show a decrease. This difference in the global average of pressure is not related to an opposite response in different models, but to the distribution of areas with positive and negative loadings in the mode of variability associated with the forcing. As shown in Fig. 5, simulations of CESM show a larger amount of areas with negative anomalies during periods with volcanic events, while simulations of GISS tend to show more areas with positive anomalies."

Figure 6 shows that simulations of GISS and CESM-LME have differences in the response of SLP during volcanic events in the regional scale. This does not contradict the conclusions extracted from the SEA, and changes in SLP during volcanic events are significant for both subensembles, as shown in Fig. 5d (more details about the significance of the SEA can be found in R1C3). We expect that the overall behavior of different climate models is similar, but this does not exclude the possibility of having important differences in their spatial patterns.

R2C14

An other example for the wind changes: "In spite of the differences in the global balance of regional positive and negative anomalies among models, all of them produce a global weakening in zonal circulation during volcanic eruptions. "

Figure 8 shows that there exist differences in the regional distribution of positive and negative winds anomalies during volcanic events in GISS and CESM-LME simulations. As clarified in R2C13, it is possible to have differences in the spatial patterns obtained with different models for SLP and winds during volcanic events but still conclude that they are impacted by changes in the forcing, as shown in Fig. 4d and 7d.

The sentence has been modified to clarify that it refers only to GISS and CESM-LME, since for the other models these maps were not presented: (P15 L19-21) "*In spite of the differences in the global balance of regional positive and negative anomalies between GISS and CESM-LME simulations, both produce a global weakening in zonal circulation during volcanic eruptions.*"

R2C15

or "In general, this global analysis shows that regional modes of variability might be indirectly influenced by external forcing".
These are descriptive assertions, which need to be quantified and evaluated in terms of significance.

The sentence has been removed.

R2C16

Based on these few examples and the overall presentation of results sections, one can conclude that the simulation changes (leading EOF and volcanoes composites) are not really significant and alternatively interpreted as mean changes, decadal and secular trends or internal variability modes acting at inter annual (such as NAO) to decadal timescales (such as SAM) depending on the authors choice. Changes in variability modes are mixed with long-term trends and mean changes. However no results are presented and assessing these various questions separately depending on the timescale.

Regarding the significance of the changes:

- The significance of MCA-LIA differences has been included in Figures 2c, 4c, 7c, 11c, 15c, 16c and 17c, showing that the changes during the transtion from MCA to LIA are significant in many areas for all the analysed variables.

- In response to R1C3, significance has been added to the SEA of volcanic events (Figures 2d, 4d, 7d, 11d, 15d, 16d and 17d). It is found that the global changes during these events are significant for most of the simulations and most of the analysed variables.

Regarding the separation of timescales:

- SEA, PC and MCA-LIA analyses for each variable are discussed in separate paragraphs, and in the methods section the scope of each analysis is described.

- In response to R2C12, the NAO, NAM and SAM indices have been computed and the evolution of the percentage of positive phases of these modes has been included in Fig. 5. This extends the conclusions obtained from the PC analysis of SLP to annual and decadal timescales.

R2C17

To sum-up I suggest major revisions. The authors need to exclude statements that are not sustained by actual relevant analyzes and focus only of long-term trends and mean MCA/LIA changes. In the actual form the paper will mislead the readers regarding the responses of the variability modes and the roles of external forcings based on speculative comments. The results presentations need to be improved focusing on specific timescale based on statistically significant signals analyzed with the appropriate method.

The text has been revised, following the previous comments, to keep only those statements directly related to the figures and analyses presented in the paper. According to R1C1, R1C17, R1C21 and R2C15, descriptive paragraphs and sentences in the results section were removed.

As commented in R1C2 and R2C12, a new figure associated with NAO, NAM and SAM was added, to support the discussion related to these modes. The selected approach allows conclusions for different timescales (with SEA, PC and MCA-LIA analyses, and now with NAO, NAM and SAM indices), and not only for the long-term.

Regarding the methodology, methods section has been completed following R1C2, R2C1, R2C4 and R2C7 to include a more detailed description of the methods and the way the significance of the changes shown with these methods is obtained.

References:

Cook, B. I., Mankin, J. S., Marvel, K., Williams, A. P., Smerdon, J. E., and Anchukaitis, K. J.: Twenty-first Century Drought Projections in the CMIP6 Forcing Scenarios, Earth's Future, https://doi.org/10.1029/2019EF001461, 2020.

Dutilleul, P., Clifford, P., Richardson, S., and Hemon, D.: Modifying the t Test for Assessing the Correlation Between Two Spatial Processes, Biometrics, 49-1, 305-314, 1993.

Huang, P., Xie, S. P., Hu, K., Huang, G., and Huang, R.: Patterns of the seasonal response of tropical rainfall to global warming, Nature Geoscience, 6, 357–361, 2013.

Luterbacher, J. et al.: European summer temperatures since Roman times, Environ. Res. Lett., 11, 024001, 2016.

Dynamical and hydrological changes in climate simulations of the last millennium

Pedro José Roldán-Gómez[1], Jesús Fidel González-Rouco[1], Camilo Melo-Aguilar[1], and Jason E. Smerdon[2]

[1]Instituto de Geociencias, Consejo Superior de Investigaciones Científicas - Universidad Complutense de Madrid, 28040 Madrid, Spain

[2]Lamont-Doherty Earth Observatory of Columbia University, Palisades, NY, United States of America

Correspondence: P. J. Roldán-Gómez (peroldan@ucm.es)

Abstract. Simulations of last millennium (LM) climate show that external forcing had a major contribution to the evolution of temperatures; warmer and colder periods like the Medieval Climate Anomaly (MCA; ca. 950-1250 CE) and the Little Ice Age (LIA; ca. 1450-1850 CE) were critically influenced by changes in solar and volcanic activity. Even if this influence is mainly observed in terms of temperatures, evidence from simulations and reconstructions show that other variables related to atmospheric dynamics and hydroclimate also were influenced by external forcing over some regions. In this work, simulations from the Coupled Model Intercomparison Project Phase 5 / Paleoclimate Modelling Intercomparison Project Phase 3 (CMIP5/PMIP3) are analyzed to explore the influence of external forcings on the dynamical and hydrological changes during the LM at different spatial and temporal scales. Principal Component (PC) analysis is used to obtain the modes of variability governing the global evolution of climate and to assess their correlation with the total external forcing at multidecadal to multicentennial timescales. For shorter timescales, a composite analysis is used to address the response to specific events of external forcing like volcanic eruptions. The results show coordinated long-term changes in global circulation patterns, which suggest expansions and contractions of the Hadley Cells and latitudinal displacements of Westerlies in response to external forcing. For hydroclimate, spatial patterns of drier and wetter conditions in areas influenced by the North Atlantic Oscillation (NAO), Northern Annular Mode (NAM) and Southern Annular Mode (SAM) and alterations in the intensity and distribution of monsoons and convergence zones are consistently found. Similarly, a clear short-term response is found in the years following volcanic eruptions. Although external forcing has a larger influence on temperatures, the results suggest that dynamical and hydrological variations over the LM exhibit a direct response to external forcing both at long and short timescales that is highly dependent on the particular simulation and model.

1 Introduction

Reconstructions and model simulations have shown that the evolution of temperatures during the last millennium (LM) was influenced both by external forcing and internal variability (Fernández-Donado et al., 2013; Schurer et al., 2013). This evolution was characterised by long-term changes, like the transition from the Medieval Climate Anomaly (MCA; ca. 950-1250 CE) to the Little Ice Age (LIA; ca. 1450-1850 CE) and during the period of anthropogenic warming. The MCA and the LIA were periods of relatively warmer and cooler conditions, respectively (Diaz et al., 2011; Graham et al., 2010), which have been related to solar variability and volcanic activity ~~responses~~ changes (Schurer et al., 2013; Mann et al., 2009), with additional contributions from ocean variability (Jungclaus et al., 2010) and ice cover feedbacks (Miller et al., 2012). After the LIA, anthropogenic activities have a major impact on most of the observed temperature changes (Masson-Delmotte et al., 2013). Temperature changes during the LM were noticeable at global scales, ~~consistently~~ consistent with changes in the global energy balance (Crowley, 2000), and at continental and large regional scales (Tardif et al., 2019; Wilson et al., 2016; Anchukaitis et al., 2017).

Because of its direct dependence on the energy balance, the response to external forcing is evident in temperature. However, coordinated changes during the LM are also found in atmospheric dynamics and hydroclimate. In extratropical areas, changes in large-scale modes of variability like the North Atlantic Oscillation (NAO) have been found both in reconstructed and simulated data (Cook et al., 2019; Trouet et al., 2009; Ortega et al., 2013). Even if for tropical areas larger uncertainties exist, long-term coordinated changes also have been found, mostly related to the variability of the El Niño - South Oscillation phenomenon (ENSO; Mann et al., 2009; Emile-Geay et al., 2013a, b).

An alteration of the circulation modes can also lead to changes in the hydroclimate of many regions. This has been found both in analyses based on reconstructed data, and to a lesser extent in analyses based on simulations (Ljungqvist et al., 2016). Reconstructions of the hydroclimate of east Africa (Anchukaitis and Tierney, 2013), Mediterranean area (Luterbacher et al., 2012), western North America (Cook et al., 2010; Steinman et al., 2013) and tropical South America (Vuille et al., 2012) show coordinated changes in the hydroclimate of the LM. The spatial pattern associated with these changes is mainly latitudinal, with latitudes of increased and decreased precipitation during the MCA and the LIA. In particular, northern Europe and northern North America showed wetter conditions during the MCA and drier during the LIA, and conversely for southern Europe and southern North America (Cook et al., 2010; Luterbacher et al., 2012). Tropical areas, like east Africa and tropical South America, also showed increased precipitation in the north during the MCA and in the south during the LIA (Anchukaitis and Tierney, 2013; Vuille et al., 2012).

Such coordinated changes in atmospheric dynamics and hydroclimate, with out-of-phase regional behavior during the MCA and LIA, are suggestive of large-scale responses to external forcing. One possibility is that changes in global temperatures, as a consequence of changes in the forcing, could have altered modes of variability, and this could have had in turn an impact on hydroclimate (Zorita et al., 2005). The latitudinal distribution of these changes both in tropical and extratropical areas is suggestive of a mechanism based on displacements of the Intertropical Convergence Zone (ITCZ) and expansions and contractions of the Hadley Cells (Newton et al., 2006; Graham et al., 2010). These changes may have contributed to the alteration of modes of variability like the NAO and Northern Annular Mode (NAM) in the Northern Hemisphere (NH) and Southern Annular Mode (SAM) in the Southern Hemisphere (SH).

To assess the influence of external forcing and internal variability on these changes, we perform analyses of simulations from the Coupled Model Intercomparison Project Phase 5 / Paleoclimate Modelling Intercomparison Project Phase 3 (CMIP5/PMIP3; Taylor et al., 2007; Stocker et al., 2013). The use of a large set of simulations generated with different models and with different boundary conditions increases the reliability of results and allows us to sample different climate sensitivities

Table 1. CMIP5/PMIP3 models analysed in this work, including the number of simulations considered in the analyses (NS), the resolution of the atmosphere and ocean components (latitude, longitude and levels), the forcing factors considered in the simulations (O = Orbital; S = Solar; V = Volcanic; G = Greenhouse gases; A = Aerosols; L = Land use and cover; according to Masson-Delmotte et al., 2013), and the references for the model experiments. All simulations span the period 850-2005 CE. This interval will be referred to herein as LM, even if within PMIP3 LM only includes 850-1850 CE. For the case of CMIP5/PMIP3 simulations, past1000 and historical experiments have been concatenated to cover this interval.

Model	NS	Res. Atm.	Res. Ocean	Forcings	References
CSIRO	1	3.2º x 5.6º - L18	1.6º x 2.8º - L21	O, S, V, G	Phipps et al. (2012)
IPSL	1	1.9º x 3.8º - L39	1.2º x 2º - L31	O, S, V, G	Dufresne et al. (2013)
MRI	1	1.9º x 3.8º - L40	0.5º x 1º - L50	O, S, V, G	Yukimoto et al. (2011); Adachi et al. (2013)
MPI	1	1.8º x 1.8º - L47	0.8º x 1.4º - L40	O, S, V, G, A, L	Giorgetta et al. (2013)
CCSM	1	1.25º x 0.9º - L26	1º x 1º - L60	O, S, V, G, A, L	Landrum et al. (2013)
HadCM	1	2.5º x 3.75º - L19	1.25º x 1.25º - L20	O, S, V, G, A, L	Tett et al. (2007)
CESM	13	2º x 2º - L26	1º x 1º - L60	O, S, V, G, A, L	Otto-Bliesner et al. (2015)
GISS	3	2º x 2.5º - L40	1º x 1.25º - L32	O, S, V, G, A, L	Schmidt et al. (2006, 2014)

and different plausible external forcing histories. Simulations from the Community Earth System Model - Last Millennium Ensemble (CESM-LME; Otto-Bliesner et al., 2015) ~~also have~~ have also been included. The use of the 13 simulations of the CESM-LME, using the same boundary conditions but with different initial conditions, allows for a systematic sampling of internal variability. With these simulations, the contribution of external forcing and internal variability to temperature, atmospheric circulation and hydroclimate has been analysed. The changes in the forcing factors during the LM incorporate both short-term changes, associated with individual volcanic events, and long-term changes, related to variations in solar activity and orbital orientation. Our analyses allow us to evaluate whether global responses in temperature, dynamics, and hydroclimate to external forcing are manifest in climate models, what is their expected spatial distribution, and whether the simulated responses are consistent with those obtained from reconstructed data.

2 Models and methods

Analyses are performed with simulations from ~~the~~ CMIP5/PMIP3, including three simulations from the Goddard Institute for Space Studies (GISS; Schmidt et al., 2006, 2014), individual LM simulations from the Community Climate System Model (CCSM; Landrum et al., 2013), the Hadley Centre Coupled Model (HadCM; Tett et al., 2007), the models of the Commonwealth Scientific and Industrial Research Organization (CSIRO; Phipps et al., 2012), the Institut Pierre Simon Laplace (IPSL; Dufresne et al., 2013), the Max Planck Institut für Meteorologie (MPI; Giorgetta et al., 2013)~~,~~ and the Meteorological Research Institute (MRI; Yukimoto et al., 2011; Adachi et al., 2013), and ~~with~~ 13 additional simulations from the CESM-LME. Some

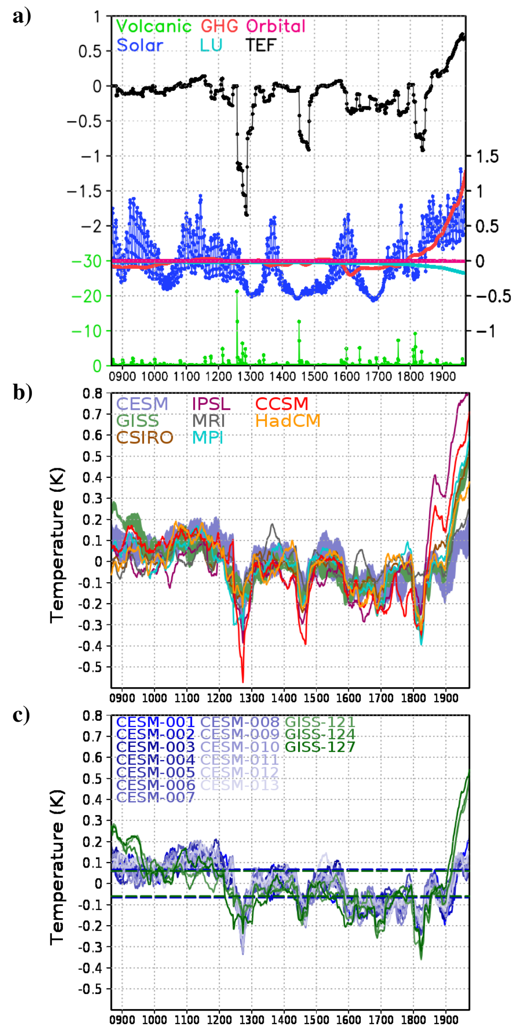

Figure 1. **(a)** External forcing factors in Wm^{-2} considered in the CESM-LME simulations, including greenhouse gases (GHG), volcanic, solar, land use and cover (LU) and orbital forcing. The CESM-LME is selected as an example since it uses standard CMIP5/PMIP3 forcing specifications (Schmidt et al., 2011, 2012). The forcing related to greenhouse gases is obtained by ~~composing~~ aggregating the contributions of CO_2, CH_4 and N_2O. Volcanic forcing is represented with a different scale (in green). An evaluation of the Total External Forcing (TEF) following Fernández-Donado et al. (2013) is also included. **(b)** Global average of temperature in the ensemble of simulations. For CESM and GISS, the range of minimum-maximum values in the subensemble at each time step is shown, instead of individual model simulations. All temperature and TEF series have been 31 years low-pass filtered with a centered moving average. **(c)** Individual simulations in CESM and GISS subensembles. Dashed blue (CESM) and green (GISS) lines represent the range ($\bar{x} \pm 2s$) of the differences between each 31-year low pass filtered member and the ensemble mean; $\bar{x}$ being the mean of the residual and s the standard deviation.

technical details of these models are summarised in Table 1, including the horizontal and vertical resolutions, the number of simulations covering the last millennium and the forcings considered in these simulations.

Even if ensembles with individual forcing factors and with reduced sets of forcings are available for some particular models, only simulations with the most complete set of external forcings that were available for each model have been considered herein. As shown in Table 1, all the analysed simulations include solar variability, volcanic eruptions, greenhouse gases and orbital changes as external forcings, while most of them also include land use and cover changes (LULC) and anthropogenic aerosols. The reconstructions of forcings considered for each simulation can be found in Masson-Delmotte et al. (2013) for the CMIP5/PMIP3 simulations and in Otto-Bliesner et al. (2015) for the CESM-LME. The forcing factors are similar in all the simulations, based on the guidelines for CMIP5/PMIP3 (Schmidt et al., 2011, 2012). The greenhouse gases are mainly obtained from MacFarling-Meure et al. (2006), the orbital changes from Berger (1978), the volcanic forcing from Gao et al. (2008) and Crowley and Unterman (2013), the solar variability from Vieira et al. (2011), Wang et al. (2005) and Steinhilber et al. (2009), the land use from Pongratz et al. (2008) and the aerosols from Lamarque et al. (2010).

Figure 1 plots the forcing factors considered in the CESM-LME simulations as an example of the LM forcings. The figure also shows an estimation of the Total External Forcing (TEF), obtained by composing the contributions of several forcing factors according to following Fernández-Donado et al. (2013) by aggregating the contributions of solar activity, orbital changes, volcanic activity, GHGs, including CO_2, CH_4 and N_2O, land use change, and anthropogenic sulfate aerosols, converted into radiative forcing units and filtered with a moving average of 31 years. TEF shows Even if it presents some limitations in the conversion of volcanic forcing and the contribution of aerosols (Fernández-Donado et al., 2013), the TEF allows analyses of the long-term evolution of the overall incoming energy, with long intervals of higher (MCA and industrial era) and lower (LIA) forcing, as well as multidecadal to centennial changes produced by the combination of solar and volcanic activity.

The response to external forcing of temperature and a number of variables representative of atmospheric circulation and hydroclimate conditions is analysed; namely sea level pressure (SLP), zonal wind (U), precipitation (P), soil moisture (SM), precipitation minus evaporation (P-E) and the Palmer Drought Severity Index (PDSI; Palmer, 1965), with the potential evapotranspiration calculated using the Thornthwaite's method (Thornthwaite, 1948). While this formulation of PDSI has been shown to be problematic for soil moisture assessments during projections of the 21st century, differences between different formulations of PDSI have been shown to be minimal over the LM interval even when the 20th century is included (Smerdon et al., 2015). Characterising the hydrological state of the soil is challenging because different General Circulation Models (GCMs) incorporate different land models and soil moisture physics. This work is focused therefore on precipitation as well as P-E as descriptors of general surface hydrological interactions, and on soil moisture and PDSI as descriptors of soil moisture content. PDSI is incorporated to employ an homogeneous description of soil moisture content across models because it is calculated from atmospheric variables and assumes the same soil parameters across all of the models. It has been defined following the self-calibrating PDSI index (scPDSI; Wells et al., 2004). All simulations have been interpolated to a common 6ºx6º grid resolution, the coarsest among the analysed simulations.

At interannual scales, some events of external forcing such as volcanic eruptions are able to explain large changes in the analysed variables (Fischer et al., 2007). To assess the impact of such events on the climate, we use a Superposed Epoch Analysis (SEA), by defining a composite with the five years before and ten years after the main volcanic eruptions within

Table 2. Correlations between the first PC of surface temperature of each model simulation and TEF (Fig. 1a) and correlations between the first PC of temperature and the PC linked to the forcing of each of the other selected variables (first PC of sea level pressure, zonal wind and scPDSI and second PC of precipitation, soil moisture and P-E) for different simulations for different simulations of the PC linked to the forcing for sea level pressure, zonal wind and precipitation (first PC of SLP and zonal wind and second PC of precipitation) with the first PC of surface temperature. Correlations of the average PC time series are also included.. Significant correlations ($p<0.05$) accounting for autocorrelation are shown in bold.

Simulation	**T / TEF**	**SLP / T**	**U / T**	**P / T**
CSIRO	**0.72**	0.26	0.33	**0.78**
IPSL	**0.71**	0.15	0.27	**0.89**
MRI	**0.65**	0.09	0.07	**0.59**
MPI	**0.72**	**0.57**	**0.46**	**0.87**
CCSM	**0.79**	**0.68**	**0.41**	**0.91**
HadCM	**0.70**	**0.35**	**0.42**	**0.82**
CESM-001	**0.61**	**0.36**	**0.54**	**0.59**
CESM-002	**0.61**	**0.41**	0.26	**0.50**
CESM-003	**0.66**	**0.46**	0.24	**0.66**
CESM-004	**0.60**	0.29	0.19	**0.57**
CESM-005	**0.61**	**0.43**	0.17	**0.56**
CESM-006	**0.65**	**0.40**	0.19	**0.58**
CESM-007	**0.66**	**0.40**	0.27	**0.62**
CESM-008	**0.65**	0.27	0.24	**0.56**
CESM-009	**0.61**	**0.36**	0.13	**0.55**
CESM-010	**0.61**	**0.53**	0.29	**0.63**
CESM-011	**0.72**	**0.49**	0.25	**0.62**
CESM-012	**0.64**	0.25	0.25	**0.64**
CESM-013	**0.63**	**0.50**	0.28	**0.64**
GISS-121	**0.64**	**0.46**	0.24	**0.88**
GISS-124	**0.67**	**0.69**	**0.56**	**0.91**
GISS-127	**0.67**	**0.46**	0.12	**0.88**
Average	**0.73**	**0.59**	**0.51**	**0.81**

the LM and computing for this composite the global average of the variables previously mentioned. Volcanic eruptions for this analysis have been the main volcanic eruptions within the LM and computing for this composite the global average of the variables previously mentioned for the five years before and ten years after the events, selected following the procedure in Masson-Delmotte et al. (2013). For simulations of CESM-LME and CCSM, the reconstruction from Gao et al. (2008) has

Table 3. Correlations for different simulations of the PC linked to the forcing for soil moisture, P-E and scPDSI (first PC of scPDSI and second PC of P-E and soil moisture) with the first PC of surface temperature and the second PC of precipitation. Correlations of the average PC time series are also included. Significant correlations ($p<0.05$) accounting for autocorrelation are shown in bold.

Simulation	**SM / T**	**P-E / T**	**scPDSI / T**	**P-E / P**	**scPDSI / P**
CSIRO	0.21	**0.65**	**0.87**	**0.76**	**0.74**
IPSL	0.02	**0.90**	-	**0.80**	-
MRI	0.07	0.33	-	**0.35**	-
MPI	0.33	**0.67**	**0.88**	**0.69**	**0.79**
CCSM	0.03	**0.77**	**0.90**	**0.80**	**0.79**
HadCM	0.08	**0.59**	-	**0.74**	-
CESM-001	0.14	**0.45**	**0.68**	**0.91**	**0.63**
CESM-002	0.10	0.28	**0.57**	**0.90**	**0.61**
CESM-003	**0.39**	**0.39**	**0.51**	**0.84**	**0.73**
CESM-004	0.03	0.29	**0.59**	**0.87**	**0.71**
CESM-005	0.07	0.33	**0.61**	**0.86**	**0.56**
CESM-006	0.19	**0.38**	**0.66**	**0.88**	**0.58**
CESM-007	0.14	**0.38**	**0.63**	**0.82**	**0.65**
CESM-008	0.05	**0.40**	**0.74**	**0.90**	**0.72**
CESM-009	0.15	0.33	**0.70**	**0.87**	**0.67**
CESM-010	0.22	0.33	**0.58**	**0.86**	**0.67**
CESM-011	0.09	**0.36**	**0.67**	**0.86**	**0.59**
CESM-012	0.16	**0.37**	**0.64**	**0.83**	**0.62**
CESM-013	0.19	**0.41**	**0.66**	**0.88**	**0.69**
GISS-121	0.17	**0.77**	**0.88**	**0.72**	**0.67**
GISS-124	0.21	**0.76**	**0.80**	**0.75**	**0.66**
GISS-127	0.32	**0.84**	**0.88**	**0.83**	**0.75**
Average	0.20	**0.62**	**0.94**	**0.93**	**0.91**

~~been considered, obtaining the minima of forcing in the years~~ which use the reconstruction from Gao et al. (2008) as volcanic forcing, the years of the composite have been selected based on the minima of forcing from this reconstruction: 1452, 1584, 1600, 1641, 1673, 1693, 1719, 1762, 1815, 1883, 1963 and 1990. For the other simulations, the reconstruction from Crowley and Unterman (2013) has been considered~~, generating a composite with the years~~: 1442, 1456, 1600, 1641, 1674, 1696, 1816, 1835, 1884, 1903, 1983 and 1992. The significance of the changes in the variables evaluated within the SEA has been calculated using a bootstrap method. 2200 sets of 12 years (100 for each simulation) have been randomly taken from the whole analysed period, excluding the years of volcanic eruptions and the ten years after them, to generate a distribution of averages for each variable. The significance of the averages computed after the 12 volcanic eruptions are then determined using the 5 and 95 confidence limits from the bootstrap distribution.

We use Principal Component (PC) analyses to describe the spatiotemporal response of variables at multidecadal to centennial timescales. The analysis has been applied to data low-pass filtered with a moving average of 31 years, in order to emphasize the response to external forcing versus internal variability (Fernández-Donado et al., 2013). We concatenate all of the low-pass filtered simulations to determine the ~~average~~ Empirical Orthogonal Functions (EOFs) across all of the models. The PCs are later obtained by projecting each individual simulation on the EOF and, to assess the agreement among different simulations, the correlation coefficients between PCs from each simulation have been computed. This method allows us to obtain the modes of variability that explain a larger percentage of variance when considering the whole ensemble, because the covariability with external forcing is expected to show common features across models and simulations.

The results presented herein have been confirmed for consistency with individual analysis of each model simulation. The ~~resulting~~ single experiment EOFs bear only regional differences that do not contradict the results obtained with the combined analyses, with spatial correlations with the multi-model EOFs reaching 0.9 for some simulations and 0.7 for most of them. The analyses have been also repeated weighting simulations so that each model would have the same influence, and the results are consistent (not shown). The concatenation of some relatively large subensembles (GISS and CESM-LME) may bias the results to these models, but ~~individual~~ these additional analyses confirm that is not the case. As an advantage, the concatenation of all simulations allows us to define EOFs that are valid for all models. Additionally, the incorporation of two subensembles allows for insights about the effects of internal variability, since the GISS and CESM ensembles incorporate identical boundary conditions and different initial conditions for each simulation.

To identify which modes from those obtained in the PC analyses are capable of showing responses to external forcing, the correlation coefficients between their associated PC time series and the first PC of temperature have been computed, and only those showing the largest correlations have been analysed in detail. The use of the first mode of temperature instead of the time series of external forcing factors removes the dependency on the particular reconstructions used by each model simulation. To confirm that the first mode of temperature is linked to the external forcing for the analysed simulations, the correlation coefficient between the PC time series associated with this mode and the respective time series of TEF used for each specific model have been computed. The significance of these correlations has been assessed with a t-test for the correlation coefficient, using an effective number of degrees of freedom that considers the window of the moving average applied to the input data.

~~Some long-term changes in the external forcing, like the one during the transition from MCA to LIA, are significant enough to be obtained not only by performing PC analyses but also by directly looking at the evolution of the variables during these two periods. To further analyse this transition,~~ For a more detailed analysis of the long-term changes during the transition from the MCA to LIA, composites for the MCA and LIA have been defined from the ensemble average of each variable~~, using the years between 950 and 1250 CE and 1450 and 1850 CE, respectively~~. The temporal phasing of these periods are regionally dependent and depend on the specific reconstruction or model (Neukom et al., 2014, 2019). For these analyses, the temporal intervals of these periods have been adopted from Masson-Delmotte et al. (2013), with the MCA ranging from 950

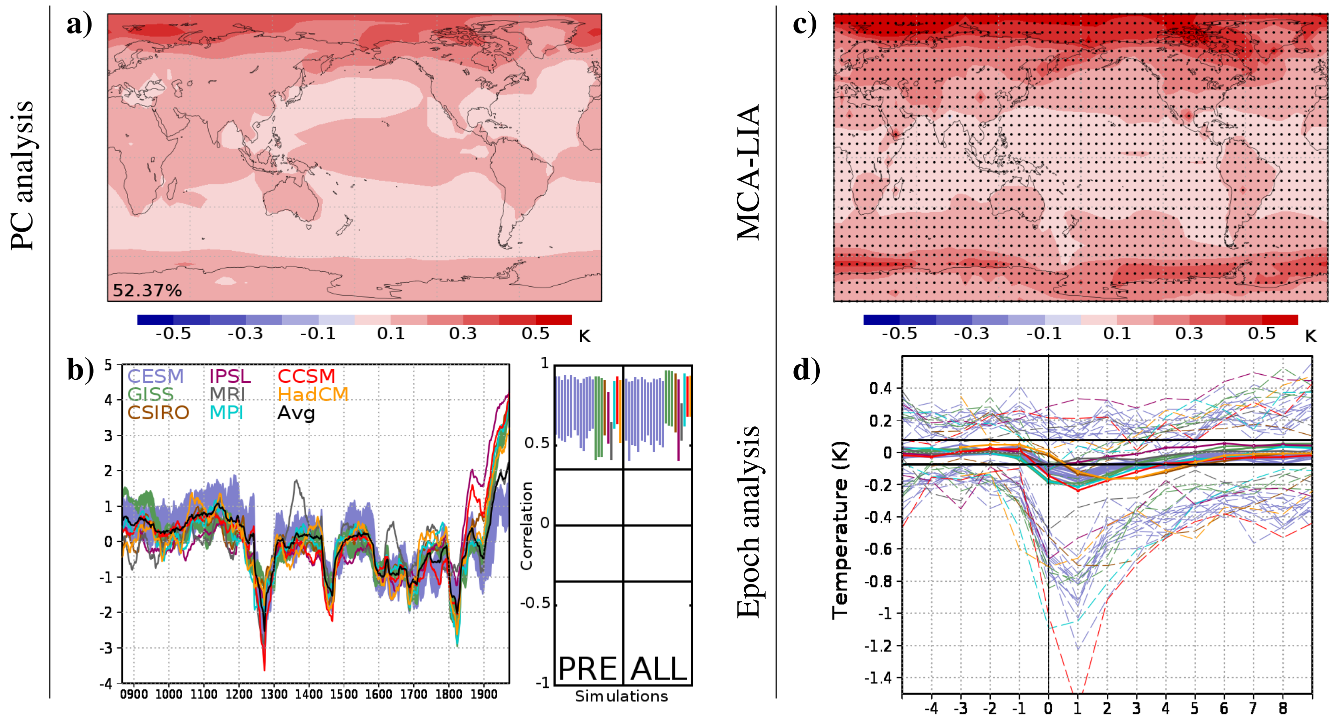

Figure 2. Analysis of temperature for the ensemble of simulations included in Table 1. **(a)** First EOF and **(b)** First PC time series for each simulation, as well as the average PC of all the simulations (black line). The percentage of explained variance is shown within the EOF map. The range of correlations between the PC of each simulation and those of other simulations is also included to the right of the plotted PCs, both for the whole period (ALL) and for the pre-industrial era (PRE). For these correlations, the significance level ($p<0.05$) accounting for autocorrelation is shown with a black line. **(c)** Map of temperature differences between MCA and LIA. Dots indicate locations where the differences are significant ($p<0.05$). **(d)** Composite average (solid line), and maxima and minima (dashed line) of global temperature anomalies in the five years before and ten years after the 12 main volcanic eruptions of the LM. Vertical line indicates the year of the volcanic event. The horizontal black lines show the significance level of the average ($p<0.10$), based on the distribution of averages of 12 years generated with 2200 sets randomly taken from the whole period, excluding the years of the 12 main volcanic eruptions and the ten years after them.

to 1250 CE, and the LIA from 1450 to 1850 CE, although these time frames may not be regionally optimal. Composite maps of the differences between these two periods are derived for temperature, SLP, zonal wind, precipitation, soil moisture, P-E and scPDSI. The significance of these MCA-LIA differences is assesed by performing a t-test for the difference of averages between the MCA and LIA for each grid point.

To better analyse the changes in the extratropical zonal circulation, the NAO, NAM and SAM indices have been computed. The NAO index has been obtained (Stephenson et al., 2006) with the difference of boreal winter (December, January and February; DJF) SLP average for (90°W to 60°E, 20°N to 55°N) and (90°W to 60°E, 55°N to 90°N), the NAM index was

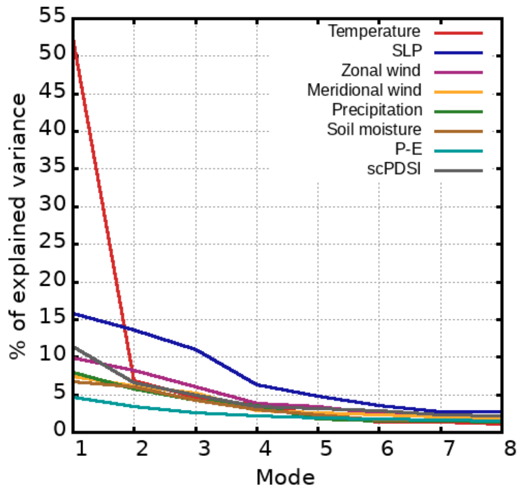

Figure 3. Percentage of variance explained by the first eight modes obtained with ~~a PC~~ the multi-model EOF analysis of temperature, SLP, zonal and meridional wind, precipitation, soil moisture, P-E and scPDSI.

calculated (Li and Wang, 2003) as the difference between the DJF zonal mean SLP at 35°N and 65°N, and the SAM index was calculated from the difference between the zonal mean of annual SLP at 40°S and 65°S (Gong and Wang, 1999). The NAO, NAM and SAM indices have been obtained for each simulation in Table 1. The average of all the simulations was subsequently computed to determine the percentage of years with positive phases for successive intervals of 50 years. The change in the percentage of positive phases from the MCA to LIA was in turn assessed and the significance of the changes evaluated using a student t-test.

3 Results

3.1 Temperature

~~Analyses based on simulations and reconstructions show that temperature during the LM experienced an evolution consistent with the temporal character of the major forcings (Zorita et al., 2005; Fernandez-Donado et al., 2013). The peaks in volcanic forcing after the main eruptions are related to periods with lower global temperatures, while the multidecadal variability and long-term trends associated with solar and anthropogenic forcings correspond with the long-term changes in temperatures that define periods of the MCA, LIA, and industrial era. This is found both at hemispheric and continental scales (Masson-Delmotte et al., 2013; Luterbacher et al., 2016; Büntgen et al., 2011; PAGES 2k Consortium, 2013), even if the temporal phasing of these periods are regionally dependent and depend on the specific reconstruction or model (Neukom et al., 2014, 2019). The temporal intervals of these periods are adopted from Masson-Delmotte et al. (2013), with the MCA ranging from 950 to 1250 CE, the LIA from 1450 to 1850 CE, and the industrial period after 1850 CE, although these time frames may not be regionally optimal.~~

Figure 1 shows global temperature averages for all the ensemble members listed in Table 1. As reported by Fernández-Donado et al. (2013) in the case of the pre-PMIP3 LM experiments, there is a quasi-linear response of temperatures to changes in external forcing, with the major warmings occurring in periods with high solar activity and GHG rise, and coolings occurring in response to lower solar forcing and increased volcanic activity. For the 20th century, all the analysed simulations consistently show a warming, but trends strongly differ among simulations due to the different climate sensitivities of each model (Vial et al., 2013) and the considered forcings (see discussion in Fernández-Donado et al., 2013). Simulations of IPSL, CCSM and GISS show a very strong trend, while simulations of CESM show a significant but smaller 20th-century temperature increase. The results for the GISS and CESM subensembles are shown in Fig. 1b by plotting the minimum-maximum spread of all subensemble members, while Fig. 1c shows, for the sake of clarity, the behavior of each subensemble member. These subensembles demonstrate that internal variability generates differences across simulations that are smaller than the differences due to structural differences in model formulation across different models. In a related and most relevant note, Figure 1c shows the range (dashed lines) of the residuals resulting from substracting the ensemble mean from each ensemble member simulation. Since the average of all ensemble members cancels out uncorrelated contributions of internal variability, the resulting ensemble mean constitues a smoothed estimation of the forced response and the residuals of substracting the ensemble mean from each ensemble member is an estimation of internal variability above 31-year timescales (Crowley, 2000; PAGES2k-PMIP3 group, 2015). Both the CESM and GISS ensembles in Fig. 1c show pre- and post-1850 low frequency changes larger than the estimated changes of internal variability. Changes in the ensemble associated with external forcing are therefore in general more relevant than those of internal variability above 31-year timescales.

A similar behaviour is found when performing a PC analysis of the simulated temperatures, as shown in Fig. 2, with the first temperature EOF and PC estimates obtained from the simulations listed in Table 1. Agreement between the different simulations is very good, all of them showing the same long-term trends described for Fig. 1. Figure 2 also shows the correlation among the estimated PCs of different simulations. Note that most of the analysed simulations show correlations larger than 0.5 and for simulations of the same model the correlations reach values around 0.9, both when analysing the whole period and when considering only the pre-industrial era. This indicates that even if the EOF has been obtained with a combined analysis, it is also representative of the individual simulations. Additionally, the use of large sets of simulations for some of the models, and in particular the use of the 13 CESM-LME simulations, does not significantly bias the results, because the correlation ranges for models with individual simulations are as large as for the others. The variance of temperature that the first PC accounts for in the ensemble is larger than 50% across all of the models, significantly larger than the variance explained by the remaining modes (Fig. 3). To evaluate whether this first mode is related to the forcing, the correlations of the PC of each simulation with the TEF (Fig. 1a) have been included in Table 2. All the correlations are significant and range between 0.61 and 0.79. The first PC of temperature is therefore mainly attributed to external forcing, and for this reason dynamics and hydroclimate variables are compared in the following sections against this mode to explore their forced responses.

Regarding the spatial pattern of the EOF, values are larger over the ice covered and continental regions and smaller over oceans. For high latitudes, this behaviour is known as the polar amplification response, and is consistent with that in climate change scenarios Regarding the spatial pattern of the EOF, values are larger over continental regions and smaller over oceans.

For high latitudes, larger values are obtained over ice covered areas, consistent with the polar amplification response in climate change scenarios (Bindoff et al., 2013). For all regions the first EOF shows positive loadings, meaning that situations of higher forcing correspond to larger temperatures for the whole planet and vice versa. This pattern has been discussed in Zorita et al. (2005) and Fernández-Donado et al. (2013), and similarities can be also observed in to the differences between the MCA and LIA (Fig. 2c). The transition from MCA to LIA in most regions leads to a decrease of simulated temperatures, consistent with the negative external forcing anomalies applied in the simulations, with a pattern of change very similar to that of the leading EOF. The MCA-LIA pattern does not emphasize the tropics as much as the EOF pattern, indicating that the low frequency variability changes in that area are minor and the higher tropical loadings in Fig. 2a stem from covariability at higher frequencies. Also note that area weighting has been applied for the EOF calculations, increasing the contribution of the tropical areas in these analyses.

At shorter timescales, the influence of external forcing is also evident. Figure 2d shows the average, maxima and minima of temperature for the composite with the five years before and ten years after the 12 main volcanic eruptions of the LM. Note that global temperature significantly decreases after these events, and their influence lasts several years until it totally disappears. There exist important differences among models in the response to volcanic eruptions. Some simulations, such as those from GISS, MPI, CESM and CCSM, show a large cooling after volcanic events that is mostly recovered after four years. However, simulations from HadCM and CSIRO show a moderate cooling that lasts for a longer period.

3.2 Atmospheric dynamics

The atmospheric circulation during the LM has been mainly analysed by focusing on modes of internal variability, such as Pacific Decadal Oscillation (PDO) and ENSO (e.g. Baek et al., 2017; Coats et al., 2016; Cook et al., 2019; Mann et al., 2009; Ortega et al., 2015; Emile-Geay et al., 2013a, b). Changes in external forcing are also likely to have had a significant impact on global atmospheric dynamics during the LM, for instance through influences on the position and size of the Hadley Cells, and therefore in the location and intensity of the large-scale modes of circulation in both hemispheres.

To evaluate some of these possible influences the possible influence of external forcing on global atmospheric dynamics, the same analyses performed for temperatures have been applied to SLP. Figure 4 shows results for the different timescales. The long-term behaviour of the first PC of pressure is similar comparable to that of the first PC of temperature. For the case of pressure, higher values are also observed during the MCA, lower values during the LIA and the average PC (black line in Fig. 4b) tends to show higher values during the MCA, lower during the LIA and a significant increase during the last century. This The similarity of the first PC of SLP with that of temperature can be quantified through the correlation coefficient values (Table 2), that are significant for 73% of the simulations in the ensemble and above 0.5 for 23% of them. The average PC correlates with a value of 0.59 (Table 2) with the corresponding PC of temperature (black line in Fig. 2b). This suggests some response to external forcing in the SLP field. The first mode accounts for only 15% of the variance in the pressure, showing an eigenvalue spectra flatter than the one of temperatures (Fig. 3). This indicates that even if there is a response to external forcing, internal variability is more relevant than in the case of temperature. Additionally, the correlations among PCs of different simulations

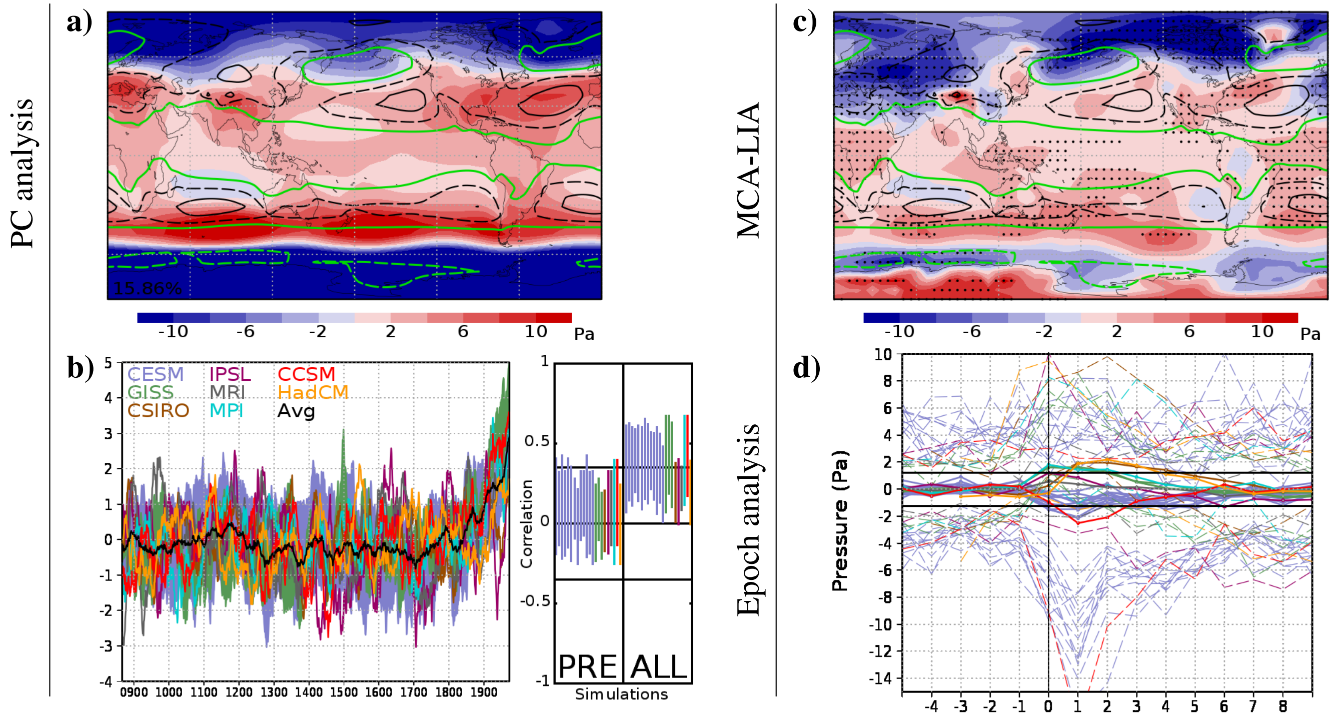

Figure 4. Analysis of SLP for the ensemble of simulations included in Table 1. **(a)** First EOF and **(b)** First PC time series for each simulation, as well as the average PC of all the simulations (black line). The percentage of explained variance is shown within the EOF map. The range of correlations between the PC of each simulation and those of other simulations is also included to the right of the plotted PCs, both for the whole period (ALL) and for the pre-industrial era (PRE). For these correlations, the significance level (p<0.05) accounting for autocorrelation is shown with a black line. **(c)** Map of SLP differences between MCA and LIA. Dots indicate locations where the differences are significant (p<0.05). Contours with climatological SLP of 986 hPa (dashed green), 1012 hPa (solid green), 1016 hPa (dashed black) and 1020 hPa (solid black) are included in the EOF and MCA-LIA maps. **(d)** Composite average (solid line), and maxima and minima (dashed line) of global SLP anomalies in the five years before and ten years after the 12 main volcanic eruptions of the LM. Vertical line indicates the year of the volcanic event. The horizontal black lines show the significance level of the average (p<0.10), based on the distribution of averages of 12 years generated with 2200 sets randomly taken from the whole period, excluding the years of the 12 main volcanic eruptions and the ten years after them.

are in general not significant over the pre-industrial period (Fig. 4b). When the whole period is considered, more significant correlations are obtained.

The EOF indicates that the first mode is mainly extratropical (Fig. 4a). In the SH, there is an increase of pressure (positive loadings) around 40º S and a decrease (negative loadings) around 80º S during the MCA (higher PC values), and conversely during the LIA. This pattern is related to the zonal SLP stratification produced by the SAM (Jones et al., 2009; Fogt et al., 2009), that responds to the long-term changes in external forcing consistently with the response in future climate change scenarios

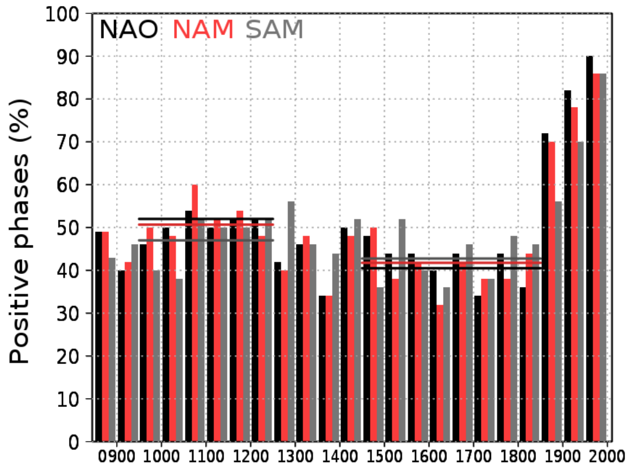

Figure 5. Percentage of years with positive NAO, NAM and SAM index for each interval of 50 years. Horizontal lines show the total percentage for the MCA and the LIA. The differences between MCA and LIA are significant with $p<0.05$ for NAO and NAM and with $p<0.15$ for SAM.

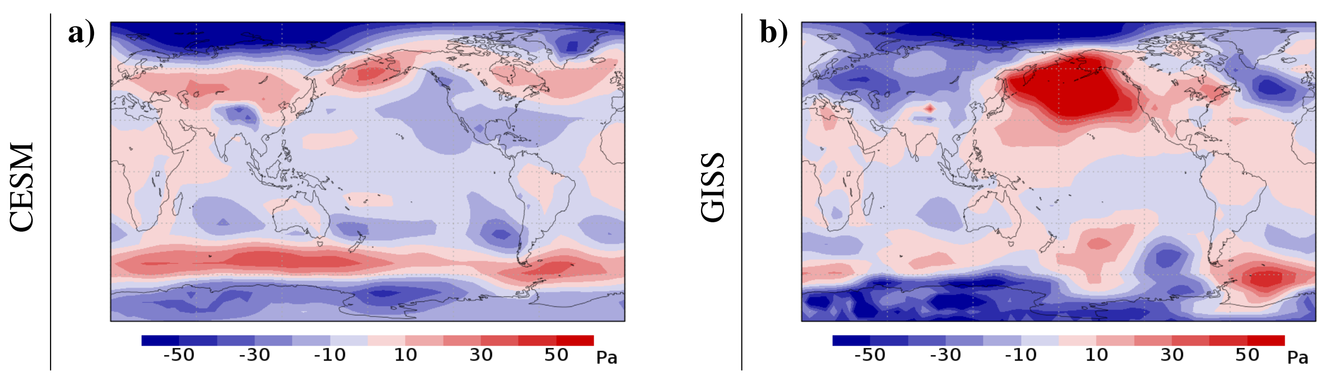

Figure 6. Maps of SLP anomalies for the 10 years after the 12 main volcanic eruptions of the LM. **(a)** Average of simulations from the CESM subensemble. **(b)** Average of simulations from the GISS subensemble.

~~(Zorita et al., 2005; Stocker et al.,2013).~~ This spatial pattern, with positive loadings over the maxima of climatological SLP (black contours of Fig. 4a) and negative loadings over the minima (green contours of Fig. 4a), contributes to the positive phase of the mode to intensify gradients between subtropical and subpolar regions. This reinforces zonal circulation and contributes to more positive phases of the SAM (Jones et al., 2009; Fogt et al., 2009), as shown in Fig. 5. Regarding the NH, the pattern of pressure associated with the first mode is not as zonal as in the SH, mostly because of the interaction with the continents. Overall, higher positive (negative) loadings distribute over subtropical (polar) regions contributing to increase (decrease) the zonal flow during the MCA and industrial period, due to the slightly higher values of the PC, also consistent with NAM

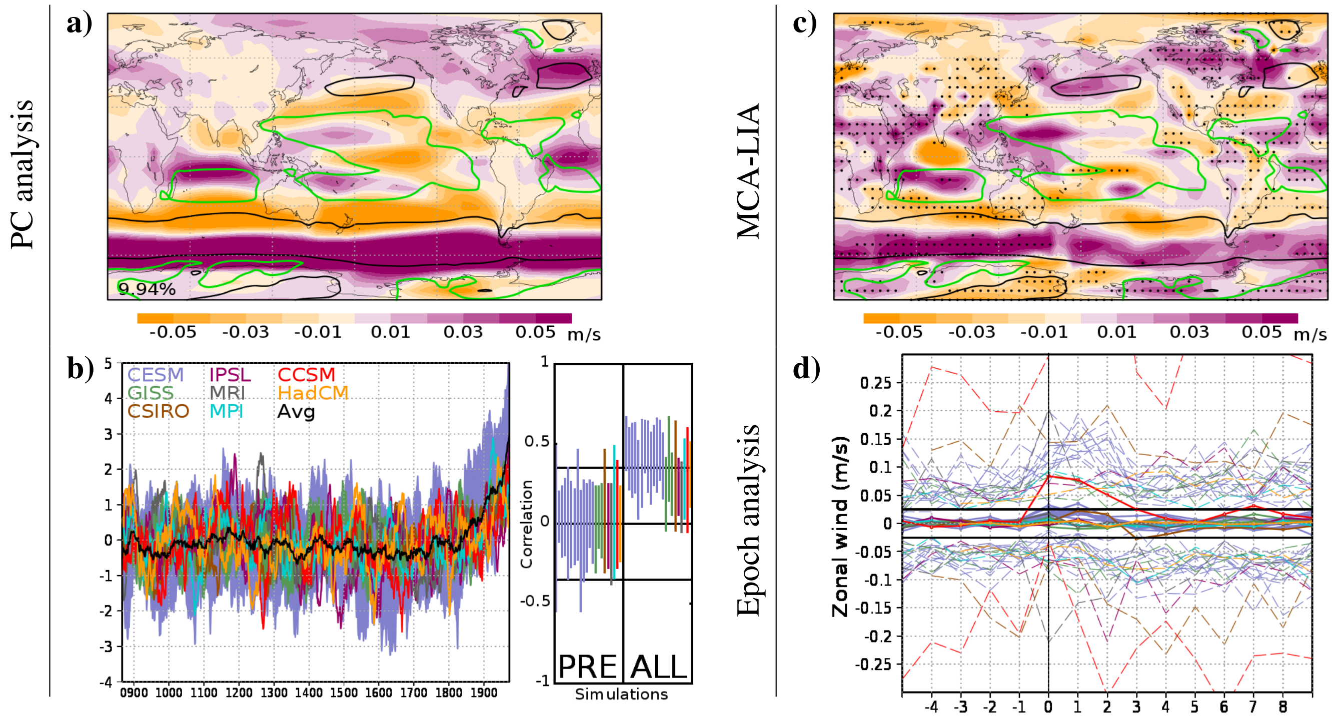

Figure 7. Analysis of zonal wind for the ensemble of simulations included in Table 1. **(a)** First EOF and **(b)** First PC time series for each simulation, as well as the average PC of all the simulations (black line). The percentage of explained variance is shown within the EOF map. The range of correlations between the PC of each simulation and those of other simulations is also included to the right of the plotted PCs, both for the whole period (ALL) and for the pre-industrial era (PRE). For these correlations, the significance level ($p<0.05$) accounting for autocorrelation is shown with a black line. **(c)** Map of zonal wind differences between MCA and LIA. Dots indicate locations where the differences are significant ($p<0.05$). Contours with climatological wind of -6 m/s (east winds; green) and 6 m/s (west winds; black) are included in the EOF and MCA-LIA maps. **(d)** Composite average (solid line), and maxima and minima (dashed line) of global zonal wind anomalies in the five years before and ten years after the 12 main volcanic eruptions of the LM. Vertical line indicates the year of the volcanic event. The horizontal black lines show the significance level of the average ($p<0.10$), based on the distribution of averages of 12 years generated with 2200 sets randomly taken from the whole period, excluding the years of the 12 main volcanic eruptions and the ten years after them.

(Thompson and Wallace, 2001) enhancement. ~~Therefore, a tendency toward more positive phases of the NAO, NAM and SAM is observed during the MCA and industrial periods.~~

~~A similar spatial pattern to that of the leading EOF is derived from a difference between the MCA and LIA periods~~ As in the leading EOF, the spatial pattern of the MCA-LIA differences (Fig. 4c) ~~A latitudinal distribution of positive and negative differences is observed, related to the intensification (MCA) and weakening (LIA) of the SAM and NAM/NAO~~ also emphasizes the latitudinal gradients. Even if the exact boundaries between areas with positive and negative MCA-LIA differences do not fully match the zonal features of the first EOF loadings, the ensemble average shows the largest differences over the subpolar and subtropical regions, which contribute to enhance the zonal flow in the MCA and weaken it during the LIA. This pattern is associated with an intensification (MCA) and weakening (LIA) of the SAM and NAM/NAO, as shown in Fig. 5. The figure shows the percentage of years with positive NAO, NAM and SAM indices for successive intervals of 50 years. Consistent with the spatial patterns and temporal evolutions shown in the PC analysis, a tendency toward more positive phases of the NAO, NAM and SAM is observed during the MCA and industrial periods.

Due to the large range of internal variability, the short-term response to volcanic forcing is not so evident in the PC of SLP as it is in the case of temperature. However, some low frequency signal is observed in the mean PC series (Fig. 4b), for which high frequencies are cancelled out. If the largest volcanic events are considered, a clearer response emerges. Figure 4d shows the global average of SLP for the composites with the five years before and ten years after the main volcanic eruptions of the LM. Note that the global average of SLP shows visible significant changes triggered by volcanic activity. The sign and magnitude of the global net changes strongly depend on the model, but there is a good agreement among simulations of the same model. For instance, simulations of GISS show an increase of pressure after volcanic events, while simulations of CESM-LME consistently show a decrease. This difference in the global average of pressure is not related to an opposite response in different models, but to the distribution of areas with positive and negative loadings in the mode of variability associated with the forcing. As shown in Fig. 6, simulations of CESM show a larger amount of areas with negative anomalies during periods with volcanic events, while simulations of GISS tend to show more areas with positive anomalies. In spite of the differences in the global balance of regional positive and negative anomalies among models, all of them between GISS and CESM-LME simulations, both produce a global weakening in zonal circulation during volcanic eruptions.

In general, this global analysis shows that regional modes of variability might be indirectly influenced by external forcing, through changes in the distribution of pressure at global scales that interact with orography and physical properties at regional and local scales. Some studies have shown that elevated forcings during the 20th century may be linked to a displacement of the ITCZ and an expansion of Hadley Cells (Lu et al., 2007; Seager et al., 2007b). These changes in the general circulation have also occurred during the MCA and LIA, and could explain the distribution of pressures in response to external forcing observed through the PC analysis and the analysis of composites. Increases in radiative forcing can produce a global warming and a significant intensification of latitudinal gradients of temperature; this intensification can generate an expansion and intensification of the Hadley Cells and a displacement of the ITCZ (Sachs et al., 2009); this expansion can further contribute to higher subtropical and lower subpolar pressures, thereby contributing to positive SAM and NAO/NAM phases.

Some studies have shown that elevated forcings during the 20th century may be linked to a displacement of the ITCZ and an expansion of Hadley Cells (Sachs et al., 2009; Lu et al., 2007; Seager et al., 2007). The position of the ITCZ and the Hadley Cells This can be described in terms of wind velocity, in which the former ITCZ is defined by the location of the Trade winds and the extension of the latter Hadley Cells is marked by the position of the Westerlies (Frierson et al., 2007). Thus, the previous analysis is also performed for the zonal wind (Fig. 7). In this case, the first mode accounts for 10% of the total variance, a smaller percentage than for the case of temperature and SLP. The average PC of zonal wind shows a correlation of 0.51 with the average PC of temperature and 0.96 with that of SLP, indicating a response to the external forcing consistent with

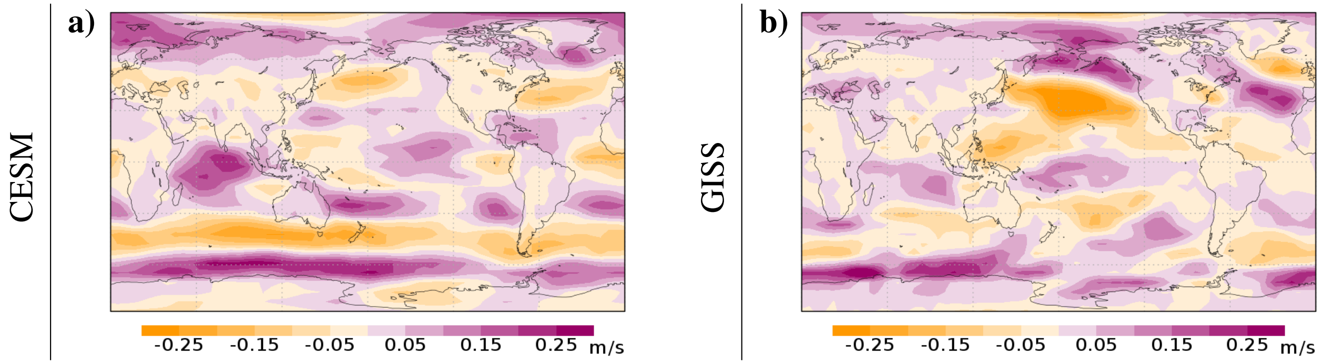

Figure 8. Maps of zonal wind anomalies for the 10 years after the 12 main volcanic eruptions of the LM. **(a)** Average of simulations from the CESM subensemble. **(b)** Average of simulations from the GISS subensemble.

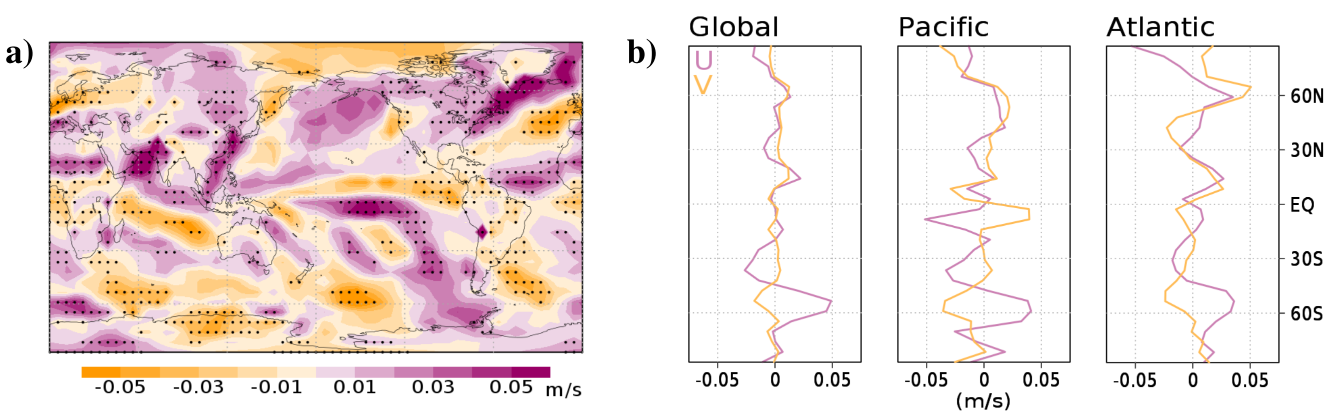

Figure 9. **(a)** Map of meridional wind differences between MCA and LIA. Dots indicate locations where the differences are significant (p<0.05). **(b)** Zonal mean of zonal wind (purple) and meridional wind (yellow) for the composite MCA-LIA, for global, central Pacific (180º W-120º W) and Atlantic (50º W-0º) basins.

the one observed in temperature and SLP. However, the correlation with the PC of temperature for the individual simulations is in general small, indicating a larger impact of internal variability. As shown in Table 2, only five simulations show significant correlations, and only two of them are larger than 0.5. The agreement among different simulations can be also assessed through the correlations among their respective PCs, which are in general not significant when the pre-industrial period is considered, and are only significant for certain simulations when they are based on the whole period (Fig. 7b). The correlation between the corresponding PC time series of zonal wind and that of SLP for each simulation is always ~~high and~~ above 0.7 ~~(p<0.05)~~.

Thus, the distribution of zonal wind in the first EOF is consistent with the distribution of pressures previously shown. ~~In situations of high forcing, such as during the MCA and the 20th century, the wind at around 30º N and 30º S decreases while~~

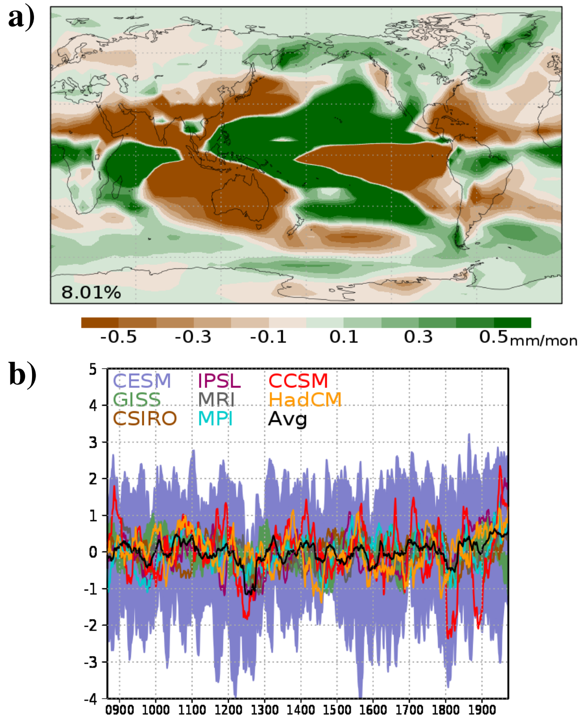

Figure 10. (a) First EOF of precipitation for the ensemble of simulations included in Table 1. The percentage of explained variance is shown within the EOF map. **(b)** PC time series for each simulation. The average of all the simulations is also included (black line).

~~the wind at around 60° N and 60° S increases. This suggests a poleward displacement of the Westerlies, consistent with the expansion of the Hadley Cells observed in the SLP analysis~~ In the positive phase of the mode, negative (positive) loadings tend to distribute over the Easterlies (Westerlies) and over their high latitude side, thus increasing latitudinal gradients and contributing to a polar displacement of the wind system; trade winds are enhanced towards higher latitudes in the Atlantic and eastern Pacific. This is consistent with an expansion of the Hadley Cell and the higher intertropical loadings and MCA-LIA anomalies in Fig. 4. The same behaviour can be observed in the composites for the MCA and LIA, where ~~the transition from the MCA to LIA is characterised by a poleward displacement of the Westerlies~~ a poleward displacement of the Westerlies is present during the simulated MCA relative to the LIA. However, the spatial pattern of the difference between the MCA and LIA differs for some regions relative to the one obtained from the EOF. For example, the differences between MCA and LIA indicate a reduction of zonal wind in the Mediterranean basin and an increase over Japan in the transition from MCA to LIA (Fig. 7c), while the loading in the EOF for these particular areas (Fig. 7a) is negative and positive, respectively.

In the short term, the behavior of zonal wind resembles that of SLP. In most simulations, the short-term noise associated with internal variability dominates over the peaks associated with volcanic eruptions, as can be observed in Fig. 7b. When composites of the main volcanic eruptions are defined (Fig. 7d), a clear influence of volcanic activity emerges. As for the case of

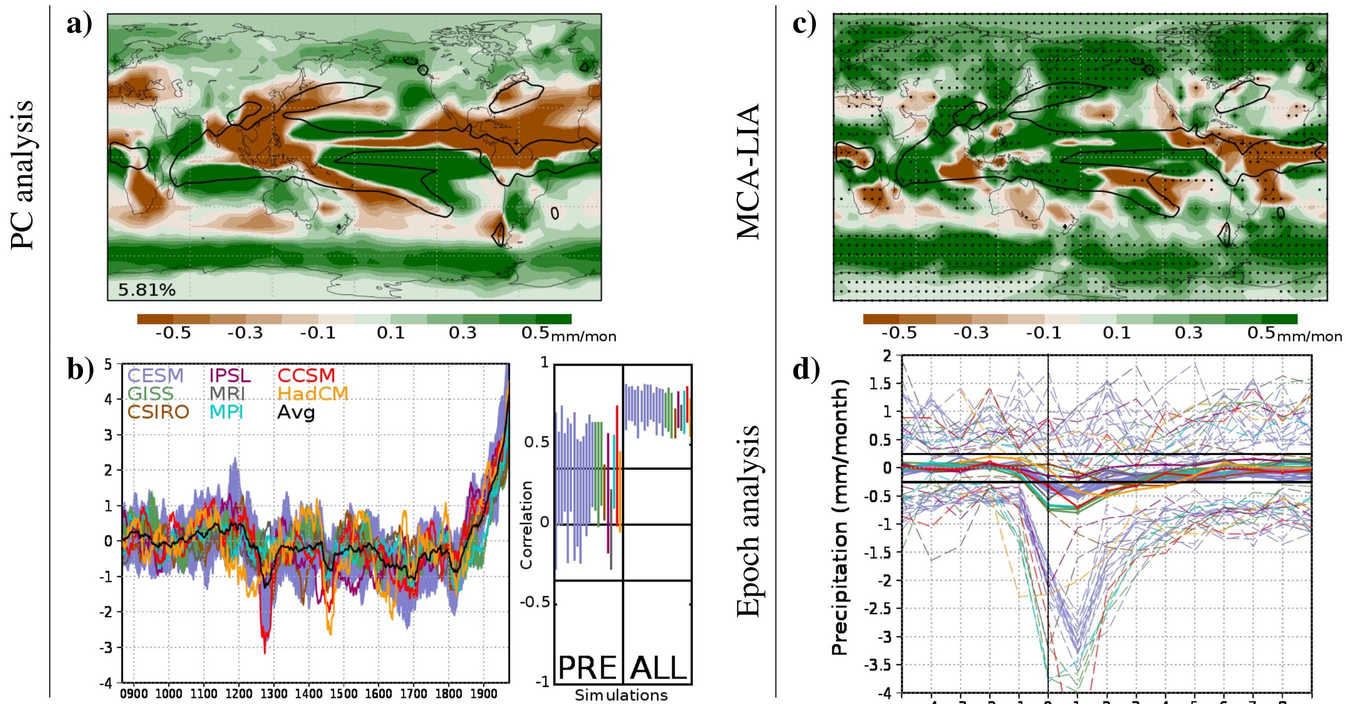

Figure 11. Analysis of precipitation for the ensemble of simulations included in Table 1. **(a)** Second EOF and **(b)** Second PC time series for each simulation, as well as the average PC of all the simulations (black line). The percentage of explained variance is shown within the EOF map. The range of correlations between the PC of each simulation and those of other simulations is also included to the right of the plotted PCs, both for the whole period (ALL) and for the pre-industrial era (PRE). For these correlations, the significance level (p<0.05) accounting for autocorrelation is shown with a black line. **(c)** Map of precipitation differences between MCA and LIA. Dots indicate locations where the differences are significant (p<0.05). Contours with climatological precipitation of 120 mm/month are included in black in the EOF and MCA-LIA maps. **(d)** Composite average (solid line), and maxima and minima (dashed line) of global precipitation anomalies in the five years before and ten years after the 12 main volcanic eruptions of the LM. Vertical line indicates the year of the volcanic event. The horizontal black lines show the significance level of the average (p<0.10), based on the distribution of averages of 12 years generated with 2200 sets randomly taken from the whole period, excluding the years of the 12 main volcanic eruptions and the ten years after them.

pressures, the sign of the impact depends on the model, mostly because of the different spatial distribution of areas with positive and negative anomalies. This can be also observed when comparing maps of zonal wind during volcanic events obtained with the CESM and GISS subensembles (Fig. 8). ~~The spatial patterns obtained with both subensembles are similar, although~~ In spite of the differences in some areas like the North and Tropical Atlantic and Pacific basins, both subensembles tend to weaken the global zonal circulation. However, the simulations of CESM (GISS) show more areas with positive (negative) zonal winds, which translate into a larger (smaller) increase of the global average. ~~For all model simulations, the pattern tends to weaken the global zonal circulation.~~

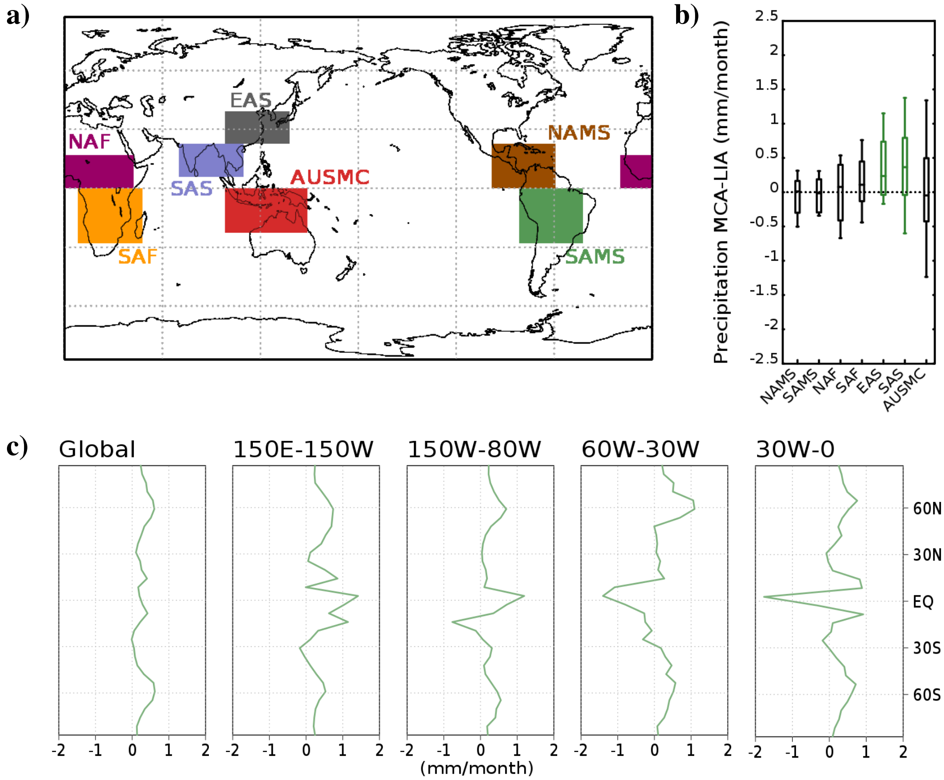

Figure 12. **(a)** Areas considered in the analysis of monsoon domains: North American Monsoon System (NAMS), South American Monsoon System (SAMS), North Africa (NAF), South Africa (SAF), East Asian Summer Monsoon (EAS), Southern Asian Summer Monsoon (SAS) and Australian-Maritime Continent (AUSMC). **(b)** Precipitation differences for MCA-LIA over the monsoon domains. Box and whisker plots show the 10th, 25th, 50th, 75th and 90th percentiles of simulations included in Table 1. Domains with significant changes ($p<0.05$) have been highlighted in green. **(c)** Zonal mean of precipitation for the composite MCA-LIA, for the whole globe and for bands of 150º E-150º W, 150º W-80º W, 60º W-30º W and 30º W-0º.

These zonal changes are also evident in the behavior of the meridional wind component. Figure 9 shows the differences between MCA and LIA in terms of meridional wind, as well as the zonal mean of these differences for zonal and meridional components, both for global and regional Pacific (180º W-120º W) and Atlantic (50º W-0º) basins (Fig. 9b). During the simulated MCA, changes in zonal and meridional winds took place with anti phase relationships that strengthened the ~~NAM and SAM~~ zonal circulation at mid and high latitudes (Fig. 9b) with increases in the NAO, NAM and SAM (Fig 5), while within the intertropical regions the Trade winds and convergence were intensified (Fig. 7c and Fig. 9). The opposite holds for the LIA.

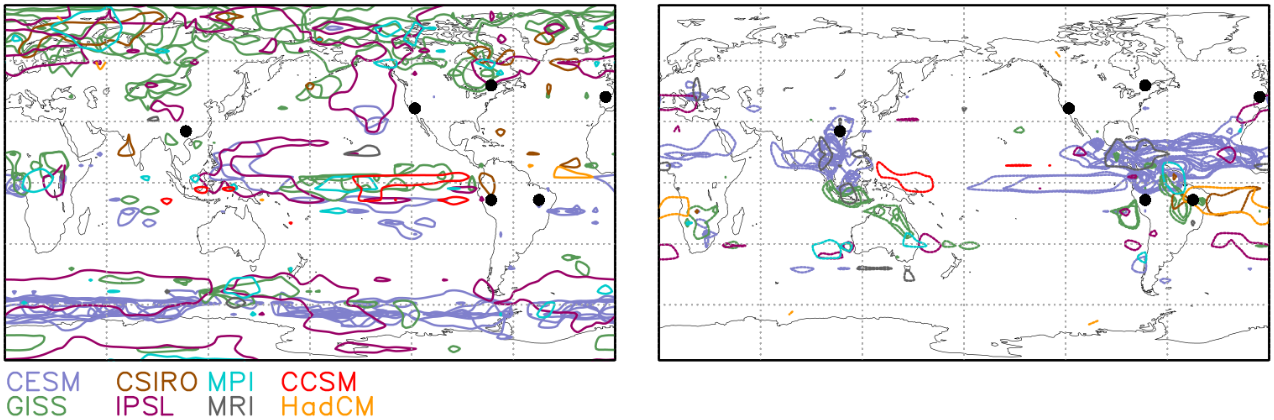

Figure 13. Regions showing high positive (left) or negative (right) correlation between precipitation and the mode of precipitation associated to the forcing for the ensemble of simulations included in Table 1. Contours of correlation equal to -0.6 and 0.6 are shown for each simulation. Dots indicate locations where the time series of Fig.14 have been extracted.

3.3 Hydroclimate

~~Previous studies related to modes of variability and teleconnections have shown that variations in the distribution of atmospheric pressure may impact the amount of precipitation over large regions (Graham et al., 2007; Seager et al., 2007a; Feng and Hu, 2008). Thus, as the external forcing has been shown to play an important role in changing the atmospheric dynamics during the LM (Sect. 3.2), it may also have a consistent influence on hydroclimate. The latter can be assessed from the same analyses performed for temperature, pressure and wind including variables of hydroclimate such as precipitation, soil moisture, scPDSI and P-E.~~

For the case of precipitation, Fig. 10 and Fig. 11 show the EOF and PC series for the leading two modes. Both modes show cross-basin influences in the tropical regions that connect the Indian, Pacific and Atlantic Oceans. Precipitation loadings are suggestive of ENSO, Pacific Decadal Oscillation (PDO) and monsoon influences (Christensen et al., 2013), thus showing large-scale coordinated responses that can connect in-phase or out-of-phase intra and inter-continent responses. Although the first PC shows large negative values during the volcanically active 13th Century and some slight increase during the 20th century, it is the second PC that resembles the external forcing response. Furthermore, its EOF emphasizes the distribution of monsoonal precipitation over the global monsoon domain within the intertropical region. In the extratropics the EOF pattern (Fig. 11a) shows distributions of loadings that are consistent with changes in NH NAM and SH SAM circulation. The PC series (Fig. 11b) clearly shows the long-term trends associated with the external forcing, with higher values during the MCA and 20th century and lower values during the LIA, as well as the short-term response to volcanic events, in agreement with the analysis of pressures (Fig. 4) and winds (Fig. 7).

There is a good agreement between different models and different simulations, with correlations larger than 0.5 for simulations of different models and reaching 0.9 for different simulations of the same model (Fig. 11b; ALL). The correlation

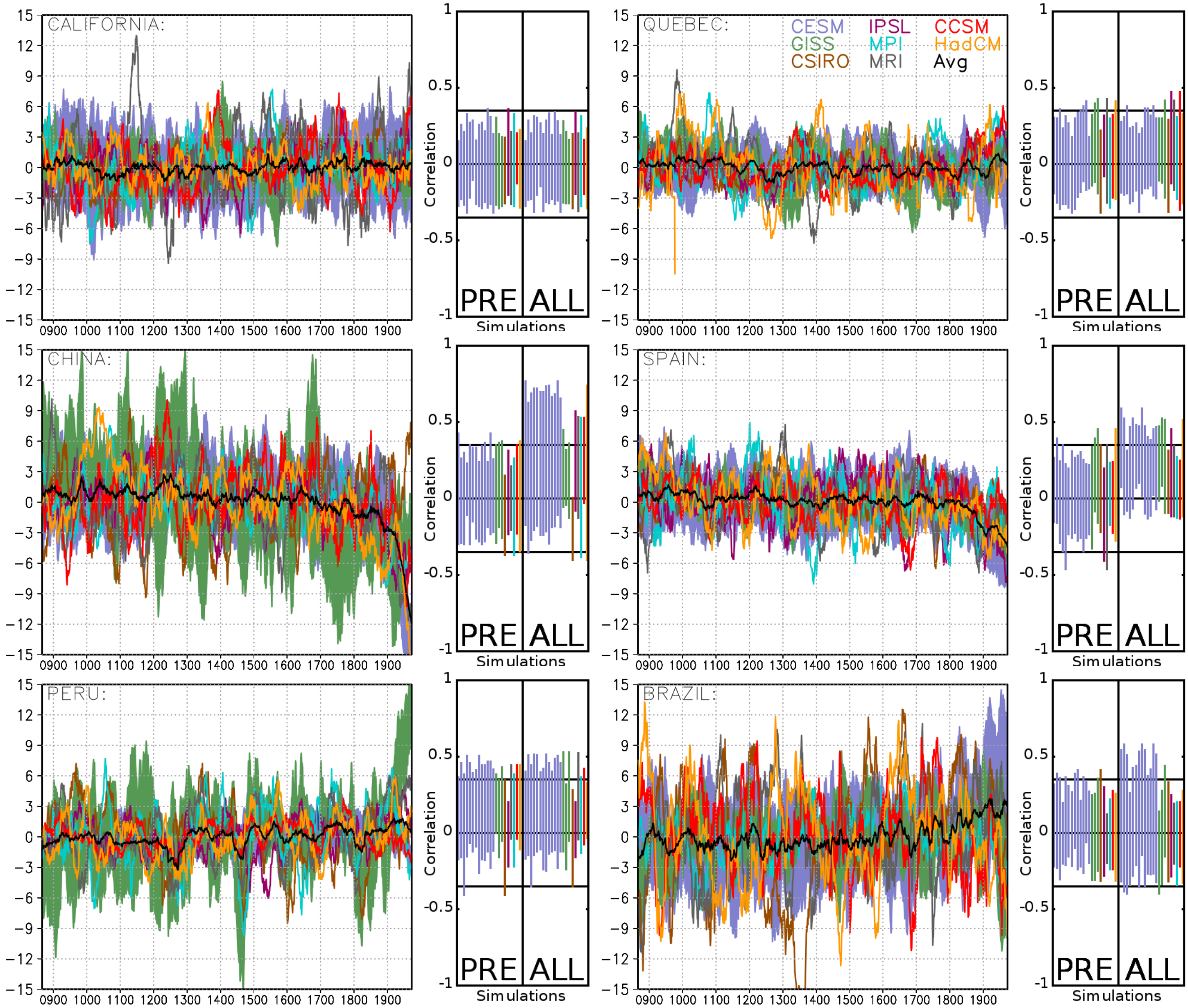

Figure 14. Time series of precipitation in mm/month for some particular case example locations. The range of correlations between the time series of each simulation and those of other simulations at those specific locations is also included, both for the whole period (right; ALL) and for the pre-industrial era (left; PRE). For these correlations, the significance level ($p<0.05$) accounting for autocorrelation is shown with a black line. All precipitation series have been 31 years low-pass filtered with a centered moving average.

between the second mode of precipitation and the first mode of temperature (Table 2) is significant for all the analysed simulations, ranging from 0.5 to 1, being higher in the simulations of GISS, IPSL and MPI and lower in the simulations of CESM and MRI. These values are larger than those obtained for pressure and winds. However, this mode accounts only for 5.8% of the precipitation variance, a lower value than the one obtained for variables of dynamics. As seen in Fig. 3, the modes associated with internal variability acquire a larger relevance in the case of precipitation. This suggests that potential detection of this signal in reconstructions would be difficult and if possible, more likely at very local scales.

The MCA-LIA differences (Fig. 11c) ~~show a similar distribution to the EOF loadings, with some regions receiving more and others less precipitation when the forcing is higher~~ show some similarities with the EOF loadings in extratropical regions, indicating larger precipitation at northern latitudes in the MCA (Fig. 11c) or with increased forcing at all timescales above 31 years (Fig. 11a,b). Within the tropical regions agreement is regionally complex, with MCA-LIA differences emphasizing low-frequency changes and EOF loadings including covariability at all timescales. Changes in dynamics described in Sect. 3.2 are consistent with the changes in precipitation. As for the case of dynamics, some zonal symmetry is observed in extratropical areas, suggesting that changes in the northern and southern annular modes affect the distribution of precipitation in these regions. The highest variability occurs in intertropical areas, over the regions with the largest amount of annual rainfall, and thus overlapping well with changes in the global monsoon domain and ITCZ convergence. ~~MCA-LIA differences show positive and negative rainfall anomalies over the~~ MCA-LIA differences are regional in scope and show anomalies of different sign over the North and South American Monsoon Systems (NAMS, SAMS; Cerezo-Mota et al., 2011; Christensen et al., 2013), therefore without a clear response of NAMS and SAMS. This agrees with uncertainty in climate change projections over the ~~North American Monsoon region~~NAMS, with CMIP5 models producing changes in precipitation that distribute around zero (Christensen et al., 2013). The same occurs over the Australian and ~~Marine~~Maritime Continent Monsoon Systems (AMSMC; Jourdain et al., 2013). ~~MCA-LIA differences show positive values~~ Positive values are found over the East Asia and Southern Asian Summer Monsoon areas (EAS, SAS; May, 2011; Boo et al., 2011), in agreement with scenario simulations (Christensen et al., 2013). Even if changes are not significant over many of these regions due to the large variability of precipitation, they show a ~~consistent pattern of response to forcing for the current generation of climate models in LM PMIP3 simulations~~ pattern of response to forcing in LM PMIP3 simulations consistent with that of scenario simulations; consistency also extends to convergence zones. In the Atlantic and eastern Pacific north of the Equator (e.g. Xie et al., 2007), ~~negative~~ positive MCA-LIA differences suggest increases in mean precipitation during the ~~LIA~~ MCA. Likewise, in the South Pacific Convergence Zone extending from the western Pacific southeastwards (e.g. Widlansky et al., 2011), ~~negative~~ positive differences also emerge, indicating increased rainfall during the MCA. Over South America, ~~rainfall shifts southeastwards and eastwards to the South Atlantic~~ negative anomalies are found in the northwest of the climatological maxima (black contours in Fig. 11b) and positive anomalies in the southeast, depicting ~~changes~~ rainfall shifts in the South Atlantic Convergence Zone (Cavalcanti and Shimizu, 2012).

To better analyse these changes, MCA-LIA precipitation differences are calculated for the monsoon domains in Fig. 12a. Changes in precipitation in the transition from the MCA to LIA (Fig. 12b) are small in NAMS and SAMS for all the analysed simulations~~, being slightly positive (negative) for NAMS (SAMS). These changes are consistent with a displacement of the convergence zone over the Americas, but important differences exist among models. Model simulations show larger discrepancies over Africa, where a clear difference between south and north is not found.~~ . Notice that over the NAMS and SAMS regions (Fig 12a) both positive and negative MCA-LIA anomalies (Fig 11c) distribute, thus hampering a clear net response. The same happens over the NAF and SAF regions with an increase in model spread and SAF being biased towards increased precipitation during the MCA. Therefore even if net regional responses are small due to compensation of anomalies of different sign, subregional differences may be large. The largest impact of MCA-to-LIA transition in the monsoon systems appears over Asia and Australia, where EAS, and SAS and AMSMC are significantly altered. Rainfall anomalies in EAS and SAS monsoon areas are larger during the MCA relative to the LIA. This pattern is consistently found in most of the simulations. For the AMSMC, some simulations show very positive differences while others are very negative, indicating that models all show important variations over this area but the magnitude and spatial distribution of these changes are strongly model dependent. The global zonal mean of precipitation for the MCA-LIA (Fig. 12c) does not show important changes but only slightly larger values of precipitation anomalies during the MCA than during the LIA for most latitudes. However, if ranges of longitude over the Pacific and Atlantic basins are considered, relevant changes in the convergence areas are observed. The zonal mean for the range of 150º E-150º W shows larger precipitation rates during the MCA relative to the LIA in equatorial areas of the central and western Pacific. In the eastern Pacific (150º W-80º W), precipitation is decreased (increased) north (south) of the Equator during the MCA-to-LIA transition, suggesting a southward displacement of the convergence zone. Ranges of 60º W-30º W and 30º W-0º show that convergence zone is also altered in the Atlantic basin, with less intense precipitation around the Equator during the MCA than during the LIA.

Figure 11d shows the global average of precipitation anomalies in the five years before and ten years after the 12 main volcanic eruptions of the LM. A consistent decrease of global precipitation can be clearly observed in all of the simulations after these volcanic events, being significant for most of them. The responses described for different timescales in Fig. 11 are consistent with changes in scenario simulations described in Christensen et al. (2013): increases in external forcing strengthen the hydrological cycle, enhancing zonal circulation in extratropical regions and increasing the global monsoon activity and equatorial convergence. This is found in the global average of precipitation after volcanic events and in the alteration of monsoons and latitudinal distribution obtained in the EOF, indicating a relevant response to external forcing in precipitation.

Figure 13 explores the robustness of regional forcing influences on precipitation across models and simulations. It shows areas of high positive correlation (above 0.6, $p<0.05$; left panel) and regions of high negative correlation (below -0.6, $p<0.05$; right panel) between precipitation and the mode of precipitation associated with the forcing of the ensemble of model simulations. All models correlate strongly Most model simulations correlate with external forcing over the same large-scale regions: the high-latitude bands related to zonal NAM and SAM circulation changes (e.g. negative correlations in the south of Europe and positive in the north) and the intertropical regions related to monsoon domains and convergence. Some models show larger areas of sensitivity to forcing while other present less regions where precipitation relates to the long-term changes in temperature produced by external forcing. For example, simulations of GISS show negative correlations in the north of Australia and the south of Africa that do not appear in simulations of CESM-LME. This shows that regardless of the agreement in the big picture, Despite most of the models showing positive correlations in the extratropical and tropical areas of the Pacific basin, and negative correlations in tropical areas of the Atlantic basin and in Southeastern Asia, the areas of high correlation are spatially very constrained to regional and even local scales and may not overlap in different models or even in simulations of the same model, this being a sign of the influence of internal variability. These regional differences are likely the sign of the important influence of internal variability. Correlations in high-latitude bands are all positive while negative correlations arise mostly

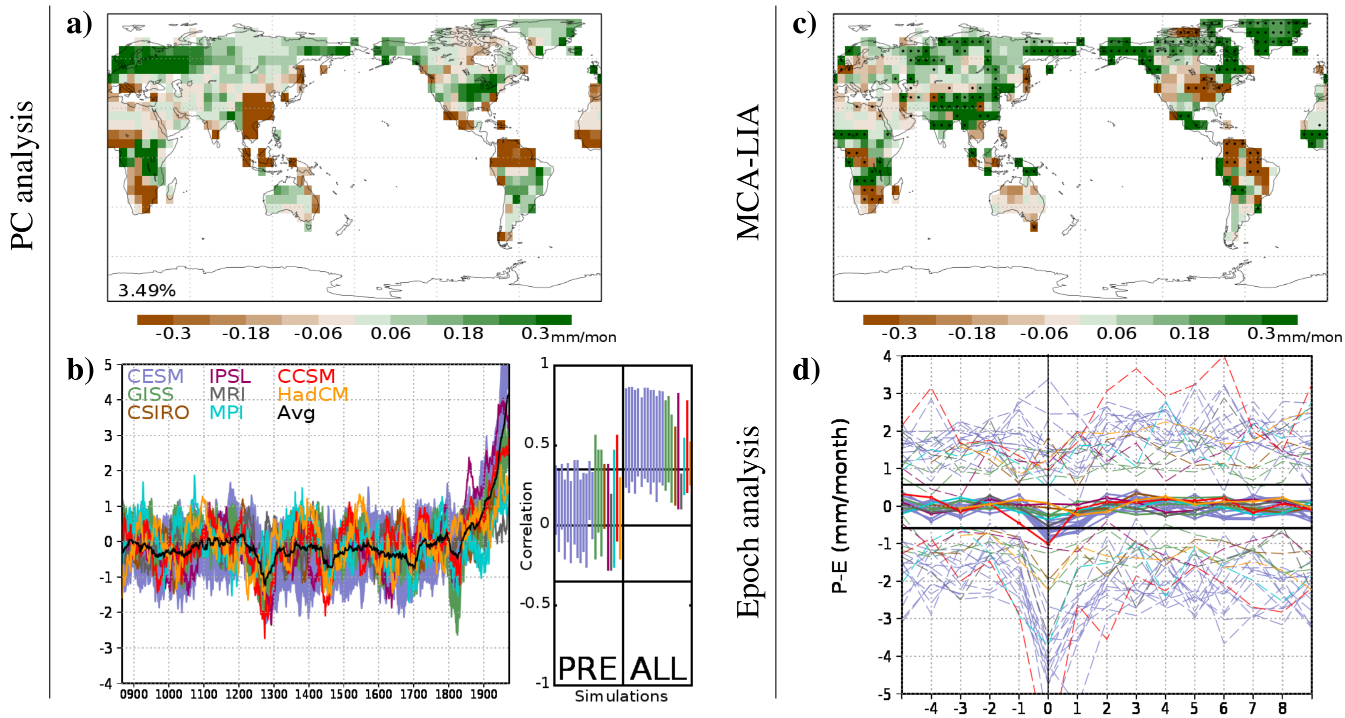

Figure 15. Analysis of P-E for the ensemble of simulations included in Table 1. **(a)** Second EOF and **(b)** Second PC time series for each simulation, as well as the average PC of all the simulations (black line). The percentage of explained variance is shown within the EOF map. The range of correlations between the PC of each simulation and those of other simulations is also included to the right of the plotted PCs, both for the whole period (ALL) and for the pre-industrial era (PRE). For these correlations, the significance level ($p<0.05$) accounting for autocorrelation is shown with a black line. **(c)** Map of P-E differences between MCA and LIA. Dots indicate locations where the differences are significant ($p<0.05$). **(d)** Composite average (solid line), and maxima and minima (dashed line) of global P-E anomalies in the five years before and ten years after the 12 main volcanic eruptions of the LM. Vertical line indicates the year of the volcanic event. The horizontal black lines show the significance level of the average ($p<0.10$), based on the distribution of averages of 12 years generated with 2200 sets randomly taken from the whole period, excluding the years of the 12 main volcanic eruptions and the ten years after them.

over the areas of monsoon activity in Africa, Asia, and America (Fig. 13 right), as in the case of negative MCA-LIA anomalies discussed above. This view has implications for detection of a potential response to global temperature and forcing changes in drought sensitive proxy data (e.g. Ljungqvist et al., 2016), as the spatial dimension of the response can be quite limited, particularly over land. Figure 14 shows examples of simulated precipitation at the gridpoint level in cases that tend to show some correlation with forcing like Spain, China, and Peru (see gridpoint locations highlighted with points in Fig. 13) and also at locations that tend to show limited connections to forcing within the ensemble: California, Quebec, and Brazil. At all these points the different ranges of internal variability tend to be larger than the forcing signal. In some areas the 20th-century trends show precipitation increases, like in the selected Brazil and Peru sites, while in others there is no response (e.g. the California

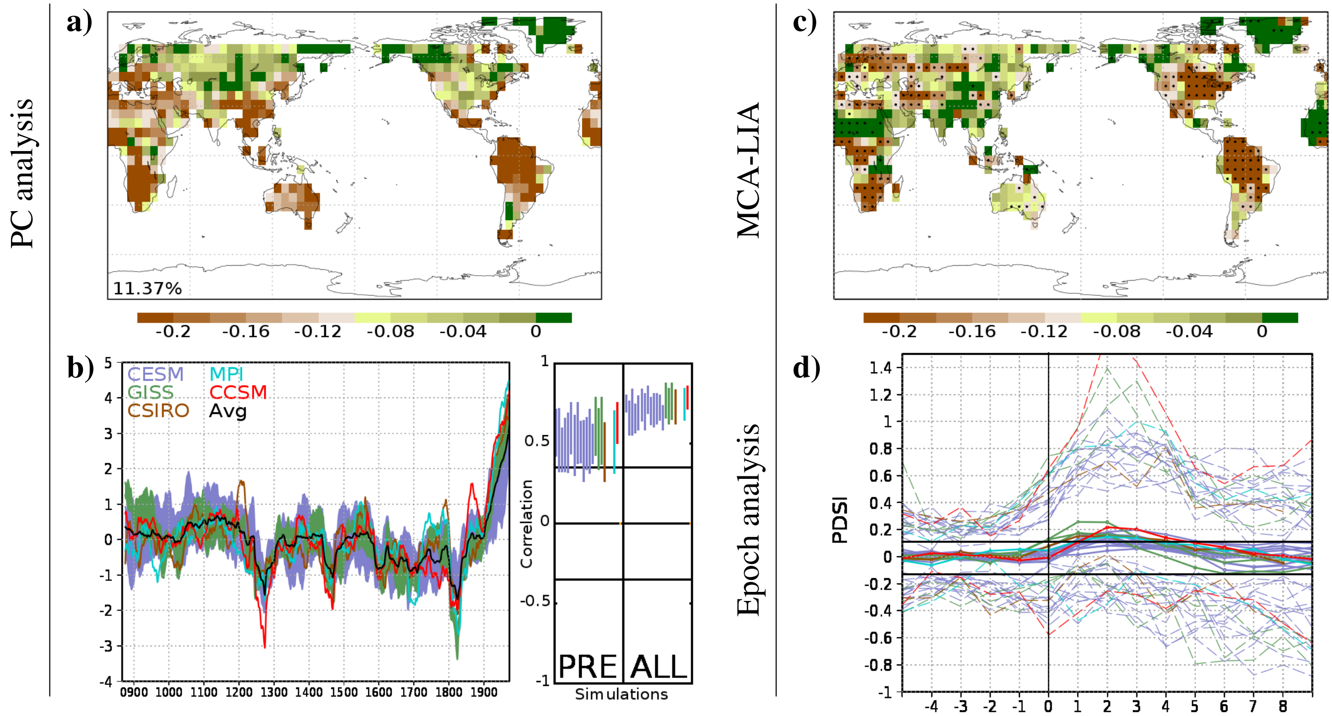

Figure 16. Analysis of scPDSI for the ensemble of simulations included in Table 1. **(a)** First EOF and **(b)** First PC time series for each simulation, as well as the average PC of all the simulations (black line). The percentage of explained variance is shown within the EOF map. The range of correlations between the PC of each simulation and those of other simulations is also included to the right of the plotted PCs, both for the whole period (ALL) and for the pre-industrial era (PRE). For these correlations, the significance level ($p<0.05$) accounting for autocorrelation is shown with a black line. **(c)** Map of scPDSI differences between MCA and LIA. Dots indicate locations where the differences are significant ($p<0.05$). **(d)** Composite average (solid line), and maxima and minima (dashed line) of global scPDSI anomalies in the five years before and ten years after the 12 main volcanic eruptions of the LM. Vertical line indicates the year of the volcanic event. The horizontal black lines show the significance level of the average ($p<0.10$), based on the distribution of averages of 12 years generated with 2200 sets randomly taken from the whole period, excluding the years of the 12 main volcanic eruptions and the ten years after them.

site) or precipitation tends to decrease (e.g. the selected sites in Spain and China). Inter-simulation correlations tend to increase during the 20th century for sites showing trends and remain insignificant for most inter-ensemble pairs in pre-industrial times.

Similar results to those obtained for precipitation are obtained when analysing other variables representative of the water content of the soil. In particular, P-E, scPDSI and soil moisture have been analysed in this work. Even if these variables provide similar information, there exist important differences between them. Because soil moisture takes into account the water balance in previous time steps, together with precipitation, evaporation and temperature, its variations are typically smoother than those observed in atmospheric variables. Something similar happens with scPDSI, which similarly takes into account soil moisture conditions from the previous months. Due to the higher number of factors considered in the computation of soil moisture and

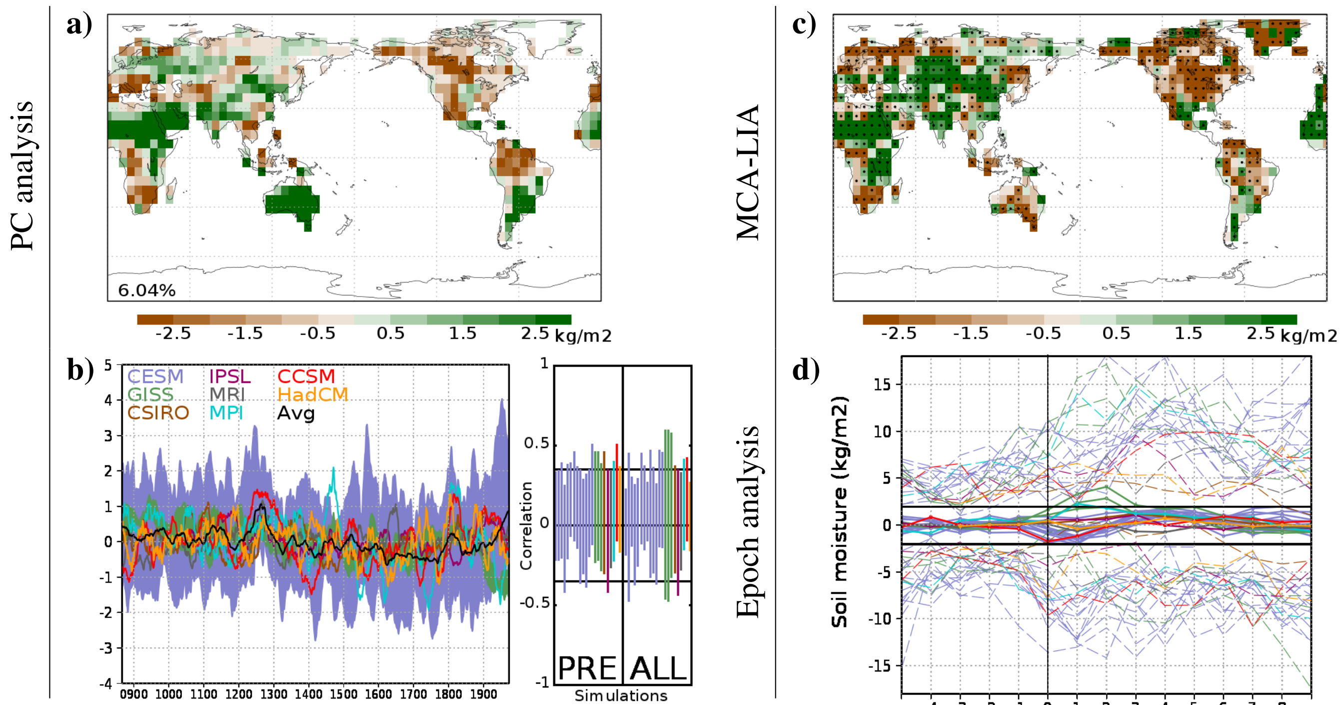

Figure 17. Analysis of soil moisture for the ensemble of simulations included in Table 1. **(a)** Second EOF and **(b)** Second PC time series for each simulation, as well as the average PC of all the simulations (black line). The percentage of explained variance is shown within the EOF map. The range of correlations between the PC of each simulation and those of other simulations is also included to the right of the plotted PCs, both for the whole period (ALL) and for the pre-industrial era (PRE). For these correlations, the significance level ($p<0.05$) accounting for autocorrelation is shown with a black line. **(c)** Map of soil moisture differences between MCA and LIA. Dots indicate locations where the differences are significant ($p<0.05$). **(d)** Composite average (solid line), and maxima and minima (dashed line) of global soil moisture anomalies in the five years before and ten years after the 12 main volcanic eruptions of the LM. Vertical line indicates the year of the volcanic event. The horizontal black lines show the significance level of the average ($p<0.10$), based on the distribution of averages of 12 years generated with 2200 sets randomly taken from the whole period, excluding the years of the 12 main volcanic eruptions and the ten years after them.

the fact that this variable is fully integrated within the models, it is a preferred variable for assessing drought variability in the models. However, different GCMs and their respective soil models may provide different treatments of soil moisture, making it difficult to combine data from different models in a single analysis. For this reason, the use of indices, such as scPDSI, may provide more consistent comparison across different models (e.g. Cook et al., 2014).

Figures 15 to 17 show the modes of P-E, scPDSI and soil moisture that bear relationship with global temperature and thus, external forcing responses. The associated mode is the second for P-E (Fig. 15) and soil moisture (Fig. 17) and the first for scPDSI (Fig. 16). P-E and scPDSI present PCs that correlate significantly with the temperature response mode (Fig. 2,

Table 3); ~~mean correlation values being~~ being the correlation of the average PC with that of temperature 0.62 and 0.94 for P-E and scPDSI, respectively. Individual correlations are significant for most simulations and particularly high for those of GISS, IPSL and CCSM. The highest correlations are attained for scPDSI, being significant and above 0.5 for all simulations, while for soil moisture correlations are smaller and in general not significant. The correlations with precipitation (Table 3) are significant for both P-E and scPDSI, being generally larger for P-E. The correlation of the average PC of P-E and scPDSI with that of precipitation reaches values of 0.93 and 0.91, respectively. For P-E and scPDSI there is a clear time response pattern that shows an evolution very similar to that of precipitation (Fig. 11) and temperature (Fig. 2), being P-E more related to precipitation and scPDSI to temperature, as shown in the correlations of Table 3. In the case of P-E, the EOF spatial pattern is similar to that of precipitation (Fig. 11a), showing large negative values over parts of the central American and north of the South American monsoon regions, as well as over the East Asian continent and over parts of the African monsoon regions, where the EOF of precipitation also includes negative loadings. Positive loadings are shown over extratropical continents, in northern Europe, southeastern North America and Alaska and eastern Siberia, thus over areas influenced by changes in zonal circulation, consistent with the results of the precipitation analyses. As in the case of precipitation, volcanic forcing produces global negative anomalies in the model ensemble that tend to last over 2-3 years.

scPDSI shows a very similar EOF pattern to that of P-E, but with larger emphasis on the negative loadings that dominate over larger scales, extending over Australia, the broader African continent, south America and large areas of North America and Eurasia (Fig. 16a). Thus, contrary to the P-E and precipitation results, which show more areas with positive anomalies during the 20th century, scPDSI shows for most regions negative trends. Negative scores in the PC during the volcanic episodes, associated to global spread negative loadings, are indicative of wetter soils, and indeed Fig. 16d shows increments in the global average of scPDSI in the model ensemble over timescales of about 5 years. Correlations between various ensemble members are high for P-E (Fig. 15b) if the 20th-century trends are considered and lower and often not significant for pre-industrial times, indicating the influence of internal variability as in the case of precipitation (Fig. 11b). scPDSI correlations are however significant and high during pre-industrial times as well, likely a sign of the influence of temperature evolution in this variable. MCA-LIA changes for P-E (Fig. 15c) are very similar to the continental component of the corresponding precipitation pattern (Fig. 11c). As in the case of the EOF loadings, Fig. 16c shows MCA-LIA changes consistent with Fig. 15c, though with widespread negative scPDSI values.

The analysis of soil moisture (Fig. 17) does not show a clear relationship to external forcing, with some of the simulations in the ensemble showing poor correlations with temperature (Table 3). Some sensitivity to volcanic events and 20th-century warming is apparent in the behavior of the PC time series. The composite of volcanic eruptions shows some increase of variability in the ensemble but not a clear response to increasing or decreasing soil moisture during volcanic events, indicating that internal variability may dominate over a potential response to the forcing. The associated EOF and MCA-LIA map (Fig. 17a,c) show similarities to those of Fig. 15a,c and 16a,c, with negative values over northern South America and parts of central and southern Africa. Over northern Africa, soil moisture shows positive loadings in the EOF and wetter values in the MCA-LIA differences. Interestingly, all EOF (MCA-LIA) maps in Fig. 15, Fig. 16 and Fig. 17 show negative (positive) values over eastern Asia and positive (negative) values over eastern North America. Despite an absence of a universal response of soil moisture to

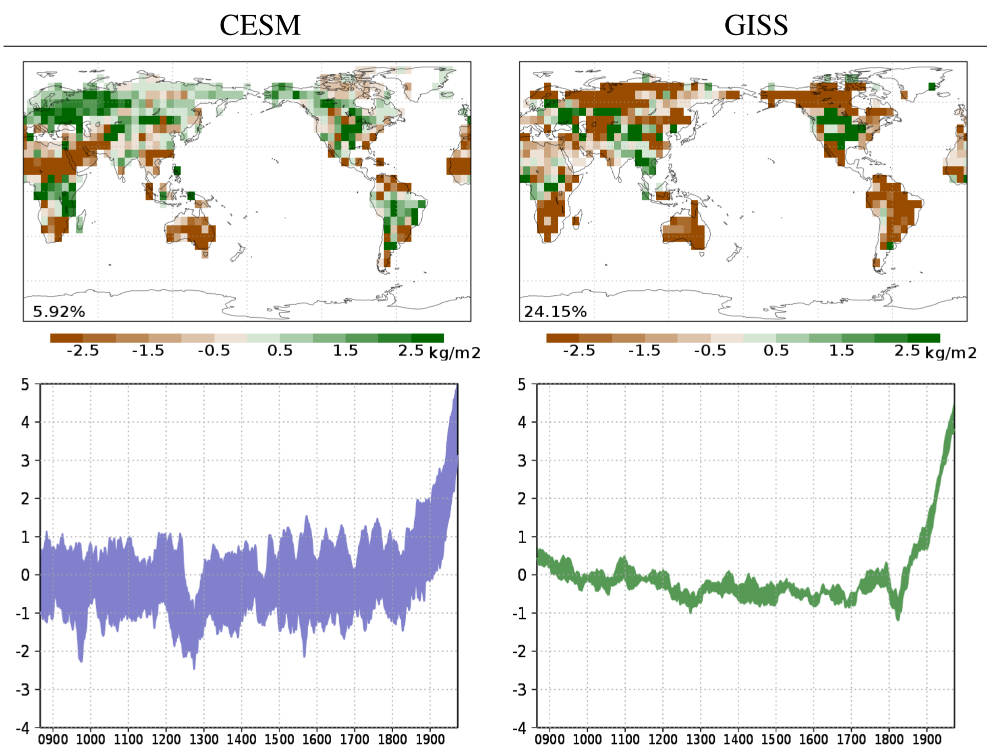

Figure 18. Second EOF and PC of soil moisture for the subensembles of CESM and GISS.

external forcing, some of the simulations ~~are~~ have clearer responses. This is the case of the CESM and GISS models. When an analysis is carried out independently for these subensembles, the resulting PC series (Fig. 18) show a clear correspondence with the temperature PC. Their corresponding EOFs show however considerable spatial differences.

These results suggest that a more focused analysis would be required to address the behaviour of drought related variables and specifically, soil moisture, also considering more ad hoc techniques and homogeneous definitions of the soil moisture content. Soil moisture, scPDSI and P-E measure different parts of the hydrological cycle. Additionally, soil moisture behavior during the 20th century may be affected by CO_2 fertilization effects (Mankin et al., 2019), which are not present on other variables such as scPDSI. For this reason, the analyses based on these variables should be considered complementary and not necessarily comparable.

4 Conclusions

This work investigated the response of the current generation of climate models to changes in external forcing during the LM. For this purpose an ensemble of ~~PMIP3/~~CMIP5/PMIP3 model simulations is considered, including all natural and anthropogenic forcings during the LM. It is focused on temperature as a reference to identify the response to external forcing and search for consistencies in the behaviour of large-scale dynamics and hydrology. Large-scale dynamics were assessed by studying changes in SLP and zonal and meridonal wind, while hydrological changes were studied by considering precipitation and drought related variables. For the latter, P-E, scPDSI and soil moisture were considered. All variables were studied considering changes at different timescales. PC analysis was used to ~~assess covariances between each variable and the temperature response and the external forcing signal at~~ identify the multi-model typical pattern of response of different variables to the external forcing changes from decadal to multicentennial timescales, MCA-LIA differences are characterized as descriptors of large-scale changes associated with changes in natural forcing during pre-industrial times and volcanic composites are used as indicators of large interannual changes.

The temperature response to forcing depicts a spatial pattern of temperature anomalies that are larger over the continents and polar areas than over oceans ~~(polar amplification)~~. The temporal response of temperature shows changes that follow those of natural forcing during the LM, and anthropogenic forcing post 1850. All analysed variables, both related to dynamics and hydroclimate, show responses that correlate or are consistent with those of temperature. Changes in SLP depict increases (decreases) of the zonal flow in the high latitudes of both hemispheres during times of higher (lower) forcing. Within the tropical regions, zonal and meridional wind components indicate that changes favour convergence and alter the monsoon system. PC time series correlate with that of temperature, and volcanic composites also show sensitivity in these variables. The responses nevertheless can be spatially variable for different models and contribute differently to global averages.

Precipitation changes show a hydrological cycle that is enhanced, consistent with the changes in temperature. At mid and high latitudes, precipitation anomalies arise in response to changes in the zonal flow. Within the intertropical regions, precipitation anomalies distribute over monsoon regions and convergence zones, consistent with the changes described for climate change scenario simulations. Such large-scale anomalies distribute over different continents, generating covariance in intra and inter-basin regions. Nevertheless, other modes of internal variability also show widespread inter-basin anomalies and have the potential to contribute to multidecadal and centennial changes in the system.

The analysis of drought related variables shows dependencies with the definition of the variable itself and its relationship to temperature or precipitation. P-E shows responses that mimic those of precipitation over the continents. Increased P-E values tend to occur with increased forcing over mid and high-latitude regions influenced by the zonal flow. Within the intertropical regions the same anomalies for precipitation are simulated over monsoon sensitive areas. ~~The pattern may change during different time intervals depending on the balance of precipitation and temperature effects as well as the effects of other modes of variability.~~ For the MCA-LIA differences, increased drought is simulated over northern South America and southern Africa monsoon regions, while increased wetness is simulated over the Asian monsoons. ~~These changes agree well with those in scPDSI MCA-LIA.~~ Unlike P-E, scPDSI shows larger correlations with temperature, with spatial patterns that show decreased wetness for most areas during the MCA and industrial period, and increased wetness during the LIA. The time evolution of its forcing response mode is very similar to that of ~~P-E~~ temperature, ~~but~~ globally ~~it produces~~ producing increased scPDSI (reduced drought) during volcanic composites and ~~contributes~~ contributing to increased drought during the 20th century.

The behaviour of soil moisture is more complex and model dependent. Some models depict clear responses to forcing but with differences in their spatial distribution and time response. The analysis of this variable shows a large dependency on the land models within the climate model itself. A response to external forcing is found when analysing subensembles of CESM and GISS independently, but not in the combined analyses including simulations from different models. This indicates that soil moisture can produce relevant results if a single model is considered, but it is not a suitable variable for analyses involving simulations with different land models.

Author contributions. This study is part of PJRG's PhD. PJRG contributed with data processing, analysis of results and writing of the paper. JFGR, CMA and JES contributed to the analysis and discussion of results and to writing the paper.

Competing interests. The authors declare that they have no conflict of interest.

Acknowledgements. We gratefully acknowledge the IlModels (CGL2014-59644-R) and GreatModelS (RTI2018-102305-B-C21) projects.

References

Adachi, Y., Yukimoto, S., Deushi, M., Obata, A., Nakano, H., Tanaka, T. Y., Hosaka, M., Sakami, T., Yoshimura, H., Hirabara, M., Shindo, E., Tsujino, H., Mizuta, R., Yabu, S., Koshiro, T., Ose, T., and Kitoh, A.: Basic performance of a new earth system model of the Meteorological Research Institute (MRI-ESM1), Papers in Meteorology and Geophysics, 64, 1–19, 2013.

Anchukaitis, K., Wilson, R., Briffa, K. R., Büntgen, U., Cook, E., D'Arrigo, R., Davi, N., Esper, J., Frank, D., Gunnarson, B. E., Hegerl, G., Helama, S., Klesse, S., Krusic, P. J., Linderholm, H. W., Myglano, V., Osborn, T. J., Zhang, P., and Zorita, E.: Last millennium Northern Hemisphere summer temperatures from tree rings: Part II, spatially resolved reconstructions, Quat. Sci. Rev., 163, 1–22, 2017.

Anchukaitis, K. J. and Tierney, J. E.: Identifying coherent spatiotemporal modes in time-uncertain proxy paleoclimate records, Clim. Dyn., 41, 1291–1306, 2013.

Berger, A.: Long-term variations of daily insolation and Quaternary climatic changes, J. Atmos. Sci., 35, 2363–2367, 1978.

Bindoff, N. L., Stott, P. A., AchutaRao, K. M., Allen, M. R., Gillett, N., Gutzler, D., Hansingo, K., Hegerl, G., Hu, Y., Jain, S., Mokhov, I. I., Overland, J., Perlwitz, J., Sebbari, R., and Zhang, X.: Detection and Attribution of Climate Change: from Global to Regional. In: Climate Change 2013: The Physical Science Basis. Contribution of Working Group I to the Fifth Assessment Report of the Intergovernmental Panel on Climate Change, Cambridge University Press, 2013.

Boo, K., Martin, G., Sellar, A., Senior, C., and Byun, Y.: Evaluating the East Asian monsoon simulation in climate models, J. Geophys. Res., 116, 2011.

Cavalcanti, I. F. A. and Shimizu, M. H.: Climate fields over South America and variability of SACZ and PSA in HadGEM2-ES, American Journal of Climate Changes, 1, 132–144, 2012.

Cerezo-Mota, R., Allen, M., and Jones, R.: Mechanisms controlling precipitation in the northern portion of the North American monsoon, J. Climate, 24, 2771–2783, 2011.

Christensen, J. H., Kanikicharla, K. K., Aldrian, E., An, S., Cavalcanti, I. F. A., Castro, M., Dong, W., Goswami, P., an d J. K. Kanyanga, A. H., Kitoh, A., Kossin, J., Lau, N., Renwick, J., Stephenson, D. B., Xie, S., and Zhou, T.: Climate phenomena and their relevance for future regional climate change. In: Climate Change 2013: The Physical Science Basis. Contribution of Working Group I to the Fifth Assessment Report of the Intergovernmental Panel on Climate Change, Cambridge University Press, 2013.

Cook, B. I., Smerdon, J. E., Seager, R., and Coats, S.: Global warming and 21st century drying, Clim. Dyn., 43, 2607–2627, 2014.

Cook, E. R., Seager, R., Heim, R. R., Vose, R. S., Herweijer, C., and Woodhouse, C.: Megadroughts in North America: placing IPCC projections of hydroclimatic change in a long-term palaeoclimate context, J. Quat. Sci, 25, 48–61, 2010.

Cook, E. R., Kushnir, Y., Smerdon, J. E., Williams, A. P., Anchukaitis, K. J., and Wahl, E. R.: A Euro-Mediterranean tree-ring reconstruction of the winter NAO index since 910 C.E., Clim. Dyn., 53, 1567–1580, 2019.

Crowley, T. J.: Causes of climate change over the past 1000 years, Science, 289, 270–277, 2000.

Crowley, T. J. and Unterman, M. B.: Technical details concerning development of a 1200 yr proxy index for global volcanism, Earth Syst. Sci. Data, 5, 187–197, 2013.

Diaz, H. F., Trigo, R., Hughes, M. K., Mann, M. E., Xoplaki, E., and Barriopedro, D.: Spatial and temporal characteristics of climate in Medieval Times revisited, Bull. Am. Meteorol. Soc., 92, 1487–1500, 2011.

Dufresne, J., Foujols, M., Denvil, S., Caubel, A., Marti, O., Aumont, O., Balkanski, Y., Bekki, S., Bellenger, H., Benshila, R., Bony, S., Bopp, L., Braconnot, P., Brockmann, P., Cadule, P., Cheruy, F., Codron, F., Cozic, A., Cugnet, D., de Noblet, N., Duvel, J., Ethe, C., Fairhead, L., Fichefet, T., Flavoni, S., Friedlingstein, P., Grandpeix, J., Guez, L., Guilyardi, E., Hauglustaine, D., Hourdin, F., Idelkadi, A., Ghattas, J., Joussaume, S., Kageyama, M., Krinner, G., Labetoulle, S., Lahellec, A., Lefebvre, M., Lefevre, F., Levy, C., Li, Z. X., Lloyd, J., Lott, F., Madec, G., Mancip, M., Marchand, M., Masson, S., Meurdesoif, Y., Mignot, J., Musat, I., Parouty, S., Polcher, J., Rio, C., Schulz, M., Swingedouw, D., Szopa, S., Talandier, C., Terray, P., Viovy, N., and Vuichard, N.: Climate change projections using the IPSL-CM5 Earth System Model: From CMIP3 to CMIP5, Climate Dyn., 40, 2123–2165, 2013.

Emile-Geay, J., Cobb, K. M., Mann, M. E., and Wittenberg, A. T.: Estimating Central Equatorial Pacific SST Variability over the Past Millennium. Part I: Methodology and Validation, Journal of Climate, 26, 2302–2328, 2013a.

Emile-Geay, J., Cobb, K. M., Mann, M. E., and Wittenberg, A. T.: Estimating Central Equatorial Pacific SST Variability over the Past Millennium. Part II: Reconstructions and implications, Journal of Climate, 26, 2329–2352, 2013b.

Fernández-Donado, L., González-Rouco, J. F., Raible, C. C., Ammann, C. M., Barriopedro, D., García-Bustamante, E., Jungclaus, J. H., Lorenz, S. J., Luterbacher, J., Phipps, S. J., Servonnat, J., Swingedouw, D., Tett, S. F. B., Wagner, S., Yiou, P., and Zorita, E.: Large-scale temperature response to external forcing in simulations and reconstructions of the last millennium, Clim. Past, 9, 393–421, 2013.

Fischer, E., Luterbacher, J., Zorita, E., Tett, S., Casty, C., and Wanner, H.: European climate response to tropical volcanic eruptions over the last half millennium, Geophys. Res. Lett, 34, L05 707, 2007.

Fogt, R. L., Perlwitz, J., Monaghan, A. J., Bromwich, D. H., Jones, J. M., and Marshall, G. J.: Historical SAM variability. Part II: Twentieth-Century variability and trends from reconstructions, observations, and the IPCC AR4 models, Am. Met. Soc., 2009.

Frierson, D. M. W., Lu, J., and Chen, G.: The width of the Hadley Cell in simple and comprehensive General Circulation Models, Geophys. Res. Lett, 2007.

Gao, C., Robock, A., and Ammann, C.: Volcanic forcing of climate over the last 1500 years: An improved ice core-based index for climate models, J. Geophys. Res., 113, D23 111, 2008.

Giorgetta, M. A., Jungclaus, J., Reick, C. H., Legutke, S., Bader, J., Böttinger, M., Brovkin, V., Crueger, T., Esch, M., Fieg, K., Glushak, K., Gayler, V., Haak, H., Hollweg, H., Ilyina, T., Kinne, S., Kornblueh, L., Matei, D., Mauritsen, T., Mikolajewicz, U., Mueller, W., Notz, D., Pithan, F., Raddatz, T., Rast, S., Redler, R., Roeckner, E., Schmidt, H., Schnur, R., Segschneider, J., Six, K. D., Stockhause, M., Timmreck, C., Wegner, J., Widmann, H., Wieners, K., Claussen, M., Marotzke, J., and Stevens, B.: Climate and carbon cycle changes from 1850 to 2100 in MPI ESM simulations for the Coupled Model Intercomparison Project phase 5, J. Adv. Model. Earth Syst., 5, 572–597, 2013.

Gong, D. Y. and Wang, S. W.: Definition of Antarctic Oscillation Index, Geophys. Res. Lett., 26, 459–462, 1999.

Graham, N. E., Ammann, C. M., Fleitmann, D., Cobb, K. M., and Luterbacher, J.: Support for global climate reorganization during the "Medieval Climate Anomaly", Clim. Dyn., 2010.

Jones, J. M., Fogt, R. L., Widmann, M., Marshall, G. J., Jones, P. D., and Visbeck, M.: Historical SAM variability. Part I: Century-Length seasonal reconstructions, Am. Met. Soc., 2009.

Jourdain, N. C., Gupta, A. S., Taschetto, A. S., Ummenhofer, C. C., Moise, A. F., and Ashok, K.: The Indo-Australian monsoon and its relationship to ENSO and IOD in reanalysis data and the CMIP3/CMIP5 simulations, Clim. Dyn., 41, 3073–3102, 2013.

Jungclaus, J., Lorenz, S., Timmreck, C., Reick, C., Brovkin, V., Six, K., Segschneider, J., Giorgetta, M., Crowley, T., and Pongraz, J.: Climate and carbon-cycle variability over the last millennium, Clim. Past, 6, 723–737, 2010.

Lamarque, J. F., Bond, T. C., Eyring, V., Granier, C., Heil, A., Klimont, Z., Lee, D., Liousse, C., Mieville, A., Owen, B., Schultz, M. G., Shindell, D., Smith, S. J., Stehfest, E., van Aardenne, J., Cooper, O. R., Kainuma, M., Mahowald, N., McConnell, J. R., Naik, V., Riahi, K., and van Vuuren, D. P.: Historical (1850-2000) gridded anthropogenic and biomass burning emissions of reactive gases and aerosols: methodology and application, Atmos. Chem. Phys., 10, 7017–7039, 2010.

Landrum, L., Otto-Bliesner, B., Wahl, E., Conley, A., Lawrence, P., Rosenbloom, N., and Teng, H.: Last Millennium Climate and its Variability in CCSM4, Journal of Climate, 1, 1085–1111, 2013.

Li, J. and Wang, J.: A modified zonal index and its physical sense, Geophys. Res. Lett., 30, doi: 10.1029/2003GL017 441, 2003.

Ljungqvist, F. C., Krusic, P. J., Sundqvist, H. S., Zorita, E., Brattström, G., and Frank, D.: Northern Hemisphere hydroclimate variability over the past twelve centuries, Nature, 532, 94–98, 2016.

Lu, J., Vecchi, G. A., and Reichler, T.: Expansion of the Hadley cell under global warming, Geophys. Res. Lett, 34, L06 805, 2007.

Luterbacher, J., García-Herrera, R., Akcer-On, S., Allan, R., Alvarez-Castro, M. C., Benito, G., Booth, J., Büntgen, U., Cagatay, N., Colombaroli, D., Davis, B., Esper, J., Felis, T., Fleitmann, D., Frank, D., Gallego, D., Garcia-Bustamante, E., Glaser, R., Gonzalez-Rouco, F., Goosse, H., Kiefer, T., Macklin, M. G., Manning, S. W., Montagna, P., Newman, L., Power, M. J., Rath, V., Ribera, P., Riemann, D., Roberts, N., Sicre, M. A., Silenzi, S., Tinner, W., Tzedakis, P. C., Valero-Garcés, B., Schrier, G., Vannière, B., Vogt, S., Wanner, H., Werner, J. P., Willett, G., Williams, M. H., Xoplaki, E., Zerefos, C. S., and Zorita, E.: A review of 2000 years of paleoclimatic evidence in the Mediterranean. In: The Climate of the Mediterranean Region: From the Past to the Future, Elsevier, 1, 87–185, 2012.

MacFarling-Meure, C., Etheridge, D., Trudinger, C., Steele, P., Langenfelds, R., van Ommen, T., Smith, A., and Elkins, J.: Law Dome CO_2, CH_4 and N_2O ice core records extended to 2000 years BP, Geophys. Res. Lett., 33, L14 810, 2006.

Mankin, J. S., Seager, R., Smerdon, J. E., Cook, B. I., and Williams, A. P.: Mid-latitude freshwater availability reduced by projected vegetation responses to climate change, Nat. Geosci., 12, 983–988, 2019.

Mann, M. E., Zhang, Z., Rutherford, S., Bradley, R. S., Hughes, M. K., Shindell, D., Ammann, C., Faluvegi, G., and Ni, F.: Global signatures and dynamical origins of the Little Ice Age and Medieval Climate Anomaly, Science, 326, 1256–1260, 2009.

Masson-Delmotte, V., Schulz, M., Abe-Ouchi, A., Beer, J., Ganopolski, A., Rouco, J. F. G., Jansen, E., Lambeck, K., Luterbacher, J., Naish, T., Osborn, T., Otto-Bliesner, B., Quinn, T., Ramesh, R., Rojas, M., Shao, X., and Timmermann, A.: Information from Paleoclimate Archives. In: Climate Change 2013: The Physical Science Basis. Contribution of Working Group I to the Fifth Assessment Report of the Intergovernmental Panel on Climate Change, Cambridge University Press, 2013.

May, W.: The sensitivity of the Indian summer monsoon to a global warming of 2ºC with respect to pre-industrial times, Clim. Dyn., 37, 1843–1868, 2011.

Miller, G. H., Geirsdóttir, A., Zhong, Y., Larsen, D. J., Otto-Bliesner, B. L., Holland, M. M. ., Bailey, D. A., Refsnider, K. A., Lehman, S. J., Southon, J. R., Anderson, C., Björnsson, H., and Thordarson, T.: Abrupt onset of the Little Ice Age triggered by volcanism and sustained by sea-ice/ocean feedbacks, Geophys. Res. Lett., 39, L02 708, 2012.

Neukom, R., Gergis, J., Karoly, D. J., Wanner, H., Curran, M., Elbert, J., González-Rouco, F., Linsley, B. K., Moy, A. D., Mundo, I., Raible, C. C., Steig, E. J., van Ommen, T., Vance, T., Villalba, R., Zinke, J., and Frank, D.: Inter-hemispheric temperature variability over the past millennium, Nature Climate Change, 4, 362–367, 2014.

Neukom, R., Steiger, N., Gómez-Navarro, J. J., Wang, J., and Werner, J. P.: No evidence for globally coherent warm and cold periods over the preindustrial Common Era, Nature, 571, 550–554, 2019.

Newton, A., Thunell, R., and Stott, L.: Climate and hydrographic variability in the Indo-Pacific Warm Pool during the last millennium, Geophys. Res. Lett., 33, L19 710, 2006.

Ortega, P., Montoya, M., González-Rouco, F., Beltrami, H., and Swingedouw, D.: Variability of the ocean heat content during the last millennium - an assessment with the ECHO-g Model, Clim. Past, 9, 547–565, 2013.

Otto-Bliesner, B. L., Brady, E. C., Fasullo, J., Jahn, A., Landrum, L., Stevenson, S., Rosenbloom, N., Mai, A., and Strand, G.: Climate variability and change since 850 C.E.: An ensemble approach with the Community Earth System Model (CESM), Bull. Am. Meteorol. Soc., 2015.

PAGES2k-PMIP3 group: Continental-scale temperature variability in PMIP3 simulations and PAGES 2k regional temperature reconstructions over the past millennium, Clim. Past Discuss., 11, 2483–2555, 2015.

Palmer, W.: Meteorologic drought, U.S. Weather Bureau, Res. Pap. No. 45, 58, 1965.

Phipps, S., Rotstayn, L., Gordon, H., Roberts, J., Hirst, A., and Budd, W.: The CSIRO Mk3L climate system model version 1.0 - Part 2: Response to external forcings, Geosci. Model Dev., 5, 649–682, 2012.

Pongratz, J., Reick, C. H., Raddatz, T., and Claussen, M.: A reconstruction of global agricultural areas and land cover for the last millennium, Global Biogeochem. Cycles, 22, GB3018, 2008.

Sachs, J. P., Sachse, D., Smittenberg, R. H., Zhang, Z. H., Battisti, D. S., and Golubic, S.: Southward movement of the Pacific intertropical convergence zone AD 1400–1850, Nature Geosci., 2, 519–525, 2009.

Schmidt, G., Ruedy, R., Hansen, J., Aleinov, I., Bell, N., Bauer, M., Bauer, S., Cairns, B., Canuto, V., Cheng, Y., Genio, A. D., Faluvegi, G., Friend, A., Hall, T., Hu, Y., Kelley, M., Kiang, N., Koch, D., Lacis, A., Lerner, J., Lo, K., Miller, R., Nazarenko, L., Oinas, V., Perlwitz, J., Perlwitz, J., Rind, D., Romanou, A., Russell, G., Sato, M., Shindell, D., Stone, P., Sun, S., Tausnev, N., Thresher, D., , and Yao, M.: Present day atmospheric simulations using GISS ModelE: Comparison to in-situ, satellite and reanalysis data, J. Climate, 19, 153–192, 2006.

Schmidt, G., Kelley, M., Nazarenko, L., Ruedy, R., Russell, G., Aleinov, I., Bauer, M., Bauer, S., Bhat, M., Bleck, R., Canuto, V., Chen, Y., Cheng, Y., Clune, T., Genio, A. D., de Fainchtein, R., Faluvegi, G., Hansen, J., Healy, R., Kiang, N., Koch, D., Lacis, A., LeGrande, A., Lerner, J., Lo, K., Matthews, E., Menon, S., Miller, R., Oinas, V., Oloso, A., Perlwitz, J., Puma, M., Putman, W., Rind, D., Romanou, A., Sato, M., Shindell, D., Sun, S., Syed, R., Tausnev, N., Tsigaridis, K., Unger, N., Voulgarakis, A., Yao, M., and Zhang, J.: Configuration and assessment of the GISS ModelE2 contributions to the CMIP5 archive, J. Adv. Model. Earth Syst., 6, 141–184, 2014.

Schmidt, G. A., Jungclaus, J. H., Ammann, C. M., Bard, E., Braconnot, P., Crowley, T., Delaygue, G., Joos, F., Krivova, N. A., Muscheler, R., Otto-Bliesner, B. L., Pongratz, J., Shindell, D. T., Solanki, S. K., Steinhilber, F., and Vieira, L. E. A.: Climate forcing reconstructions for use in PMIP simulations of the Last Millennium (v1.0), Geosci. Model Dev., 4, 33–45, 2011.

Schmidt, G. A., Jungclaus, J. H., Ammann, C. M., Bard, E., Braconnot, P., Crowley, T., Delaygue, G., Joos, F., Krivova, N. A., Muscheler, R., Otto-Bliesner, B. L., Pongratz, J., Shindell, D. T., Solanki, S. K., Steinhilber, F., and Vieira, L. E. A.: Climate forcing reconstructions for use in PMIP simulations of the Last Millennium (v1.1), Geosci. Model Dev., 5, 185–191, 2012.

Schurer, A. P., Hegerl, G. C., Mann, M. E., Tett, S. F. B., and Phipps, S. J.: Separating forced from chaotic climate variability over the past millennium, J. Climate, 26, 6954–6973, 2013.

Seager, R., Ting, M., Held, I., Kushnir, Y., Lu, J., Vecchi, G., Huang, H., Harnik, N., Leetmaa, A., Lau, N., Li, C., Velez, J., and Naik, N.: Model projections of an imminent transition to a more arid climate in Southwestern North America, Science, 316, 1181–1184, 2007.

Smerdon, J. E., Cook, B. I., Cook, E. R., and Seager, R.: Bridging Past and Future Climate across Paleoclimatic Reconstructions, Observations, and Models: A Hydroclimate Case Study, Journal of Climate, 28, 3212–3231, 2015.

Steinhilber, F., Beer, J., and Fröhlich, C.: Total solar irradiance during the Holocene, Geophys. Res. Lett., 36, L19 704, 2009.

Steinman, B. A., Abbott, M. B., Mann, M. E., Stansell, N. D., and Finney, B. P.: 1,500 year quantitative reconstruction of winter precipitation in the Pacific Northwest, Proc. Natl. Acad. Sci., 109, 11 619–11 623, 2013.

Stephenson, D., Pavan, V., Collins, M., Junge, M., and Quadrelli, R.: North Atlantic Oscillation response to transient greenhouse gas forcing and the impact on European winter climate: A CMIP2 multi-model assessment, Clim. Dyn., 27, 401–420, 2006.

Stocker, T. F., Qin, D., Plattner, G. K., Alexander, L. V., Allen, S. K., Bindoff, N. L., Bréon, F. M., Church, J. A., Cubasch, U., Emori, S., Forster, P., Friedlingstein, P., Gillett, N., Gregory, J. M., Hartmann, D. L., Jansen, E., Kirtman, B., Knutti, R., Kumar, K. K., Lemke, P., Marotzke, J., Masson-Delmotte, V., Meehl, G. A., Mokhov, I. I., Piao, S., Ramaswamy, V., Randall, D., Rhein, M., Rojas, M., Sabine, C., Shindell, D., Talley, L. D., Vaughan, D. G., and Xie, S. P.: Technical Summary. In: Climate Change 2013: The Physical Science Basis. Contribution of Working Group I to the Fifth Assessment Report of the Intergovernmental Panel on Climate Change, Cambridge University Press, 2013.

Tardif, R., Hakim, G. J., Perkins, W. A., Horlick, K. A., Erb, M. P., Emile-Geay, J., Anderson, D. M., Steig, E. J., and Noone, D.: Last Millennium Reanalysis with an expanded proxy database and seasonal proxy modeling, Clim. Past, 15, 1251–1273, 2019.

Taylor, C. M., Parker, D. J., and Harris, P. P.: An observational case study of mesoscale atmospheric circulations induced by soil moisture, Geophys. Res. Lett., 34, L15 801, 2007.

Tett, S., Betts, R., Crowley, T., Timothy, J., Johns, C., Jones, A., Osborn, T., Öström, E., Roberts, D., and Woodage, M.: The impact of natural and anthropogenic forcings on climate and hydrology since 1550, Clim. Dynam., 28, 3–34, 2007.

Thompson, D. W. J. and Wallace, J. M.: Regional Climate Impacts of the Northern Hemisphere Annular Mode, Science, 293, 85–89, 2001.

Thornthwaite, C. W.: An approach toward a rational classification of climate, Geogr. Rev., 38, 55–94, 1948.

Trouet, V., Esper, J., Graham, N. E., Baker, A., Scourse, J. D., and Frank, D. C.: Persistent Positive North Atlantic Oscillation Mode Dominated the Medieval Climate Anomaly, Science, 324, 78, 2009.

Vial, J., Dufresne, J. L., and Bony, S.: On the interpretation of inter-model spread in CMIP5 climate sensitivity estimates, Clim. Dyn., 41, 3339–3362, 2013.

Vieira, L. E. A., Solanki, S. K., Krivova, N. A., and Usoskin, I.: Evolution of the solar irradiance during the Holocene, Astron. Astrophys., 531, A6, 2011.

Vuille, M., Burns, S. J., Taylor, B. L., Cruz, F. W., Bird, B. W., Abbott, M. B., Kanner, L. C., Cheng, H., and Novello, V. F.: A review of the South American Monsoon history as recorded in stable isotopic proxies over the past two millennia, Clim. Past, 2012.

Wang, Y., Cheng, H., Edwards, R. L., He, Y., Kong, X., An, Z., Wu, J., Kelly, M. J., Dykoski, C. A., and Li, X.: The Holocene Asian monsoon: links to solar changes and North Atlantic climate, Science, 308, 854, 2005.

Wells, N., Goddard, S., and Hayes, M. J.: A self-calibrating Palmer Drought Severity Index, Journal of Climate, 17, 2335–2351, 2004.

Widlansky, M. J., Webster, P. J., and Hoyos, C. D.: On the location and orientation of the South Pacific Convergence Zone, Clim. Dyn., 36, 561–578, 2011.

Wilson, R., Anchukaitis, K., Briffa, K. R., Büntgen, U., Cook, E., D'Arrigo, R., Davi, N., Esper, J., Frank, D., Gunnarson, B., Hegerl, G., Helama, S., Klesse, S., Krusic, P. J., Linderholm, H. W., Myglano, V., Osborn, T. J., Rydval, M., and Zorita, E.: Last millennium northern hemisphere summer temperatures from tree rings: Part I: The long term context, Quat. Sci. Rev., 134, 1–18, 2016.

Xie, P., Miyama, T., Wang, Y., Xu, H., de Szoeke, S. P., Small, R. J. O., Richards, K. J., Mochizuki, T., and Awaji, T.: A regional ocean-atmosphere model for eastern Pacific climate, Journal of Climate, 20, 1504–1522, 2007.

Yukimoto, S., Yoshimura, H., Hosaka, M., Sakami, T., Tsujino, H., Hirabara, M., Tanaka, T. Y., Deushi, M., Obata, A., Nakano, H., Adachi, Y., Shindo, E., Yabu, S., Ose, T., and Kitoh, A.: Meteorological Research Institute - Earth System Model Version 1 (MRI-ESM1) - Model Description, Tech. Rep. of the Met. Res. Inst., 64, 2011.

Zorita, E., González-Rouco, J. F., von Storch, H., Montávez, J. P., and Valero, F.: Natural and anthropogenic modes of surface temperature variations in the last thousand years, Geophys. Res. Lett, 32, L08 707, 2005.